

1 **Species-specific molecular barriers to SARS-CoV-2 replication in bat cells**

2

3 Sophie-Marie Aicher^{1,2}, Felix Streicher^{1,2}, Maxime Chazal¹, Delphine Planas^{3,4}, Dongsheng Luo⁵,

4 Julian Buchrieser³, Monika Nemcova⁶, Veronika Seidlova⁶, Jan Zukal⁷, Jordi Serra-Cobo⁸, Dominique

5 Pontier^{9,10}, Olivier Schwartz^{3,4}, Jiri Pikula⁶, Laurent Dacheux^{5*}, Nolwenn Jouvenet^{1*}

6

7

8 ¹ Virus Sensing and Signaling Unit, Department of Virology, Institut Pasteur, UMR3569 CNRS, Paris, France

9 ² Université de Paris, Paris, France

10 ³ Virus and Immunity Unit, Department of Virology, Institut Pasteur, UMR3569 CNRS, Paris, France

11 ⁴ Vaccine Research Institute, Créteil, France

12 ⁵ Lyssavirus Epidemiology and Neuropathology Unit, Institut Pasteur, Paris, France

13 ⁶ Department of Ecology and Diseases of Zoo Animals, Game, Fish and Bees, University of Veterinary Sciences

14 Brno, Brno, Czech Republic

15 ⁷ Institute of Vertebrate Biology of the Czech Academy of Sciences Brno, Czech Republic

16 ⁸ Institut de Recerca de la Biodiversitat (IRBio), Faculty of Biology, University of Barcelona, Barcelona, Spain

17 ⁹ Université de Lyon, LabEx Ecofect, Lyon, France

18 ¹⁰ Université Lyon 1, CNRS, Laboratoire de Biométrie et Biologie Evolutive UMR5558, Villeurbanne, France

19

20

21 *co-corresponding/co-senior authors

22

23 Short title: SARS-CoV-2 replication in bat cells

24

25 **Abstract**

26 Bats are natural reservoirs of numerous coronaviruses, including the potential ancestor of SARS-
27 CoV-2. Knowledge concerning the interaction between coronaviruses and bat cells is sparse. We
28 investigated the susceptibility of primary cells from *Rhinolophus ferrumequinum* and *Myotis* species,
29 as well as of established and novel cell lines from *Myotis myotis*, *Eptesicus serotinus*, *Tadarida*
30 *brasiliensis* and *Nyctalus noctula*, to SARS-CoV-2 infection. None of these cells were sensitive to
31 infection, not even the ones expressing detectable levels of angiotensin-converting enzyme 2 (ACE2),
32 which serves as the viral receptor in many mammalian species. The resistance to infection was
33 overcome by expression of human ACE2 (hACE2) in three cell lines, suggesting that restriction to
34 viral replication was due to a low expression of bat ACE2 (bACE2) or absence of bACE2 binding in
35 these cells. Infectious virions were produced but not released from hACE2-transduced *M. myotis* brain
36 cells. *E. serotinus* brain cells and *M. myotis* nasal epithelial cells expressing hACE2 efficiently
37 controlled viral replication. This ability to control viral replication correlated with a potent interferon
38 response. Our data highlight the existence of species-specific molecular barriers to viral replication in
39 bat cells. These novel chiropteran cellular models are valuable tools to investigate the evolutionary
40 relationships between bats and coronaviruses.

41

42 **Author summary**

43 Bats host ancestors of several viruses that cause serious disease in humans, as illustrated by the
44 on-going SARS-CoV-2 pandemic. Progress in investigating bat-virus interactions have been hampered
45 by a limited number of bat cell lines. We have generated primary cells and cell lines from several bat
46 species that are relevant for coronavirus research. The varying susceptibilities of the cells to SARS-
47 CoV-2 infection offered the opportunity to uncover some species-specific molecular restrictions to
48 viral replication. All bat cells exhibited a potent entry-dependent restriction. Once this block was
49 overcome by over-expression of human ACE2, which serves at the viral receptor, two bat cell lines
50 controlled well viral replication, which correlated with the inability of the virus to counteract antiviral
51 responses. Other cells potently inhibited viral release. Our novel bat cellular models contribute to a
52 better understanding of the molecular interplays between bats and viruses.

53

54 **Introduction**

55 Bats are natural hosts of numerous coronaviruses, including members of the *Betacoronavirus*
56 genus, which comprises viruses belonging to the severe acute respiratory syndrome coronavirus
57 (SARS-CoV) 1 and 2 lineages [1,2]. The RaTG13 virus, which shares 96.1% nucleotide sequence with
58 SARS-CoV-2 [3], was sampled from faeces of *Rhinolophus affinis* in the Yunnan province of China in
59 2013[4]. RmYN02 virus, which also belongs to the RaTG13/SARS-CoV-2 lineage, was recently
60 identified in *Rhinolophus malayanus* collected in China [1]. Other viruses belonging to this lineage
61 have been recently identified in *Rhinolophus* bats sampled in Thailand [5] and in Cambodia [6].
62 SARS-CoV-2 related coronaviruses (SC2r-CoVs) are thus probably widely distributed in South-East
63 Asia. In addition, numerous other bat species worldwide are infected with betacoronaviruses,
64 including species of the *Myotis*, *Nyctalus*, *Tadarida* and *Eptesicus* genera [7–12].

65 The risk of spillback transmission of SARS-CoV-2 from humans to domestic animals or wildlife
66 remains a major concern, as this reverse zoonotic transmission has been already documented in pet
67 animals, tigers and gorillas in zoos, and farmed minks [13,14]. Given the likely bat origin of SARS-
68 CoV-2, bats could be putatively at risk of spillback transmission [15]. The establishment of novel bat
69 reservoirs would have a severe impact on wild-life conservation and public health measures.

70 Betacoronaviruses circulating in bats and humans use the surface receptor angiotensin-converting
71 enzyme 2 (ACE2) to enter cells [4,16–18]. Viral binding to ACE2 is followed by the proteolytic
72 cleavage of the viral spike (S) proteins by either the plasma-membrane resident transmembrane
73 protease serine 2 (TMPRSS2) or the endosomal cathepsin L (CTSL)[19]. This cleavage is mandatory
74 for the fusion between the viral and cellular membranes. Thus, localization and expression of
75 TMPRSS2 and CTSL dictate whether the virus enters cells by fusing at the cell surface or in
76 endosomes [19].

77 Several approaches have been used to predict the ability of ACE2 from phylogenetically diverse
78 bat species to promote viral entry. First, comparison of ACE2 protein sequences from 37 bat species,
79 including species of the genus *Rhinolophus*, predicted a low or very low ability to interact with viral S
80 proteins[20]. Second, expressing ACE2 from dozen bat species in non-permissive mammalian cells

81 using genuine viruses or pseudo-viruses carrying SARS-CoV-2 S proteins revealed that ACE2 from
82 *Rhinolophus*, *Myotis* and *Eptesicus* species allowed viral entry [21–24], albeit often less efficiently
83 than human ACE2. However, these approaches using *in silico* analysis or ectopic expression of bat
84 ACE2 in human or hamster cells do not allow to draw conclusions as to which bat species might
85 support SARS-CoV-2 replication. Other factors unique to bat cells may potentially modulate viral
86 entry and replication. Indeed, experiments performed with cells derived from lung tissue of
87 *Rhinolophus alcyone* and *Myotis daubentonii* showed that they were not susceptible to infection with
88 vesicular stomatitis viruses (VSV) bearing SARS-CoV-2 S proteins [17]. Cells originating from lung
89 and kidney tissue of *Rhinolophus sinicus* and *Eptesicus fuscus* were not permissive to SARS-CoV-2
90 either [25,26]. These studies underline the limitation of predicting the ability of S proteins to bind
91 ACE2 orthologs based on computational models or ectopic expression.

92 Only a handful of models are available to study the replication of betacoronaviruses in bat cells.
93 Viral replication was detected in *Rhinolophus sinicus* lung and brain cells, as well as in *Pipistrellus*
94 *abramus* kidney cells [27], but viral titers were very low. By contrast, SARS-CoV-2 replicated
95 efficiently in *R. sinicus* intestinal organoids [28], confirming further the susceptibility of *Rhinolophus*
96 cells to the virus. Intranasal inoculation of SARS-CoV-2 in *Rousettus aegypticus* resulted in transient
97 infection of their respiratory tract and oral shedding of the virus [29], indicating that bats unrelated to
98 the *Rhinolophus* genus are also susceptible to the virus. Since the manipulation of bat organoid and
99 animal models remains challenging, there is a need to develop cell lines from various organs and
100 species to gain deeper insights into bat-virus co-evolution [30]. Here, we developed novel cellular
101 models derived from bat species circulating widely in Europe and Asia. The varying susceptibilities of
102 the cells to SARS-CoV-2 infection offered the opportunity to uncover some species-specific molecular
103 restrictions to viral replication.

104

105 **Results**

106 **Resistance to SARS-CoV-2 infection in selected bat cell lines**

107 Species belonging to the *Rhinolophus* genus, including *R. ferrumequinum*, are known natural
108 hosts for numerous SARS-CoV-related betacoronaviruses [9,31]. Alphacoronaviruses [10,32,33], and

109 possibly betacoronaviruses [8], circulate in species belonging to the *Myotis* genera. Primary cells
110 generated from wing biopsies of *R. ferrumequinum*, *M. myotis*, *M. nattereri* and *M. brandtii* (table 1)
111 were subjected to infection by SARS-CoV-2 at a multiplicity of infection (MOI) of 1. Flow cytometry
112 analyses were performed using anti- S antibodies at 24 hours post-infection (hpi). Vero E6 cells,
113 which are African green monkey kidney cells known to be susceptible to SARS-CoV-2 [34] were used
114 as positive controls. Around 40% of Vero E6 cells were positive for the viral S protein (Fig. 1A-B).
115 Neither *R. ferrumequinum* or *Myotis* spp. primary cells were susceptible to SARS-CoV-2 (Fig. 1A-B).
116 We then tested the susceptibility of previously described cell lines generated from *Eptesicus serotinus*
117 [35], *Myotis myotis* [36] and *Tadarida brasiliensis* (table 1) to SARS-CoV-2. *E. serotinus* cells were
118 isolated from brain (FLG) and kidney (FLN) [35](table 1). *M. myotis* cells were established from brain
119 (MmBr), tonsil (MmTo), peritoneal cavity (MmPca), nasal epithelium (MmNep) and nervus
120 olfactorius (MmNol)[36] (table 1). Tb1lu cells are *T. brasiliensis* lung cells. We also generated
121 *Nyctalus noctula* cell lines from lung (NnLu), liver (NnLi) and kidney (NnKi) (table 1).
122 Betacoronaviruses have been sampled in species belonging to these 4 bat genus [8–12]. Human
123 intestinal Caco-TC7 cells and human lung A549 cells, which are both representative of tissues targeted
124 by the virus in infected patients [37], were used as controls. All cells were infected with SARS-CoV-2
125 at a MOI of 1. Around 23% of Caco-TC7 cells were positive for the viral S protein at 24 hpi (Fig. 1C-
126 D). None of the other selected cells were susceptible to SARS-CoV-2 (Fig. 1C-D).

127 SARS-CoV-2 variants exhibiting diverse mutations in the S protein have emerged at the end of
128 2020, leading to increased transmissibility or/and immune escape in humans [38,39]. The so-called
129 ‘B.1.351/20H/501Y.V2’ and ‘P1/20J/501Y.V3’ variants, which first appeared in South-Africa and
130 Brazil, respectively, have acquired the ability to efficiently replicate in mice airways [40]. We tested
131 the susceptibility of the selected bat cells and Caco-TC7 cells to these two variants. Flow cytometry
132 analysis performed at 24 hpi revealed that none of the bat cell lines were positive for S proteins (Fig.
133 S1A-B). By contrast, the two variants replicated in Caco-TC7 cells (Fig. S1A). Thus, neither the initial
134 virus nor recently emerged variants are able to replicate in the 13 selected bat cell lines.

135 The lack of production of viral protein in the primary bat cells and bat cell lines, as well as in
 136 A549 cells, could be explained by the absence of one or several key pro-viral factor(s) and/or the
 137 presence of potent antiviral factor(s).

	Bat species	Common name	Family	Organ	Transformation method	Reference
16104	<i>Rhinolophus ferrumequinum</i>	greater horseshoe bat	<i>Rhinolophidae</i>	Skin (patagium)	None – primary cell	This study
29B	<i>Myotis myotis</i>	Common serotine bat	<i>Vespertilionidae</i>	Skin (patagium)	None – primary cells	This study
19PL50	<i>Myotis nattereri</i>	Natterer's bat	<i>Vespertilionidae</i>	Skin (patagium)	None – primary cells	This study
MBra10	<i>Myotis brandtii</i>	Brandt's bat	<i>Vespertilionidae</i>	Skin (patagium)	None – primary cells	This study
FLG-ID	<i>Eptesicus serotinus</i>	Common serotine bat	<i>Vespertilionidae</i>	Brain	Immortalized FLG-R cells with SV40 large T antigen	CCLV-RIE 1152
FLG-R	<i>Eptesicus serotinus</i>	Common serotine bat	<i>Vespertilionidae</i>	Brain	Natural	CCLV-RIE 1093
FLN-ID	<i>Eptesicus serotinus</i>	Common serotine bat	<i>Vespertilionidae</i>	Kidney	Immortalized FLN-R cells with SV40 large T antigen	CCLV-RIE 1134
FLN-R	<i>Eptesicus serotinus</i>	Common serotine bat	<i>Vespertilionidae</i>	Kidney	Natural	CCLV-RIE 1091
MmBr	<i>Myotis myotis</i>	Greater mouse-eared bat	<i>Vespertilionidae</i>	Brain	SV40 large T antigen	He et al., 2014
MmNep	<i>Myotis myotis</i>	Greater mouse-eared bat	<i>Vespertilionidae</i>	Nasal epithelium	SV40 large T antigen	He et al., 2014
MmNol	<i>Myotis myotis</i>	Greater mouse-eared bat	<i>Vespertilionidae</i>	Nerve	SV40 large T antigen	He et al., 2014
MmPca	<i>Myotis myotis</i>	Greater mouse-eared bat	<i>Vespertilionidae</i>	Macrophage	SV40 large T antigen	He et al., 2014
MmTo	<i>Myotis myotis</i>	Greater mouse-eared bat	<i>Vespertilionidae</i>	Tonsil	SV40 large T antigen	He et al., 2014
NnKi	<i>Nyctalus noctula</i>	Common noctule	<i>Vespertilionidae</i>	Kidney	SV40 large T antigen	This study
NnLi	<i>Nyctalus noctula</i>	Common noctule	<i>Vespertilionidae</i>	Liver	SV40 large T antigen	This study
NnLu	<i>Nyctalus noctula</i>	Common noctule	<i>Vespertilionidae</i>	Lung	SV40 large T antigen	This study
Tb1Lu	<i>Tadarida brasiliensis</i>	Mexican/Brazilian free-tailed bat	<i>Molossidae</i>	Lung	Natural?	CCLV-RIE 0072

138

139 **Table 1. Overview of bat primary cells and cell lines used in the study.**

140

141 **Expression of endogenous ACE2 and ectopically-expressed hACE2 in bat cell lines**

142 To determine whether the absence or low expression of ACE2 was the main limiting factor for
 143 SARS-CoV-2 replication in the selected bat cell lines, we first evaluated the level of ACE2 expression
 144 by RT-qPCR analysis. Levels of ACE2 were above the detection limit in FLG-R, MmTo, MmPca,
 145 MmNol cells and in the three Nn cells (Fig. 2A). These cells do not however support viral replication
 146 (Fig. 1C-D). Thus, S proteins may have a low affinity for ACE2 expressed in these cells. They may
 147 also be deficient in expression of both TMPRSS2 and CTSL. To test this hypothesis, viral input was
 148 treated with the serine-protease trypsin to activate the S protein and allow viral fusion in a TMPRSS2-

149 and CTSL-independent manner [19], at the surface of NnKi cells, which express the highest level of
150 ACE2 of all bat cells (Fig. 2A). Trypsin-treated virions did not replicate better than non-treated virions
151 in Caco-T7 (Fig. S1C), suggesting that pre-activation of S proteins does not affect viral fusion in these
152 cells. NnKi cells were resistant to infection with trypsin-treated virions (Fig. S1C), suggesting that S
153 cleavage is not the factor limiting viral infection in these cells.

154 We then stably expressed hACE2 in bat and A549 cells using lentiviral transduction. Six of the 13
155 bat cell lines, representing three species (*Myotis myotis*, *Nyctalus noctula* and *Eptesicus serotinus*)
156 tolerated the lentiviral transduction and antibiotic selection. We used RT-qPCR, Western blot and flow
157 cytometry to analyze hACE2 expression in these cell lines. The transduced cells displayed different
158 hACE2 expression profile (Fig. 2B-D). RT-qPCR analysis revealed that hACE2 mRNA abundances
159 were higher in all transduced cells than in Caco-TC7 cells (Fig. 2B), which support SARS-CoV-2
160 replication (Fig. 1C-D and Fig. S1A). This suggests that transduced cells express hACE2 at a level
161 high enough to permit viral entry. In line with the RT-qPCR analysis, Western blot analysis showed
162 that MmBr-ACE2 cells expressed the highest level of hACE2 among all transduced cell lines (Fig.
163 2C). ACE2 was barely detectable in Caco-TC7 cells (Fig. 2B). A faint band was also detected in non-
164 transduced NnKi cells, likely representing endogenous bACE2. This suggests that *N. noctula* ACE2 is
165 recognized by the antibody raised against hACE2 in this assay and that Nnki cells expressed higher
166 levels of ACE2 than lung and liver cells from the same bat. These data are in line with the RT-qPCR
167 analysis of endogenous ACE2 expression (Fig. 2A). Flow cytometry analysis revealed that around
168 80% of MmBr-ACE2 cells and 15% of FLG-ID-ACE2 brain cells were positive for hACE2 (Fig. 2D).
169 On average, 1-2% of A549-ACE2 and MmNep-ACE2 cells were positive for hACE2 and even less Nn
170 cells were expressing hACE2 (Fig. 2D). These low percentages were surprising in light of the RT-
171 qPCR and Western blot data (Fig. 2B and 2C). However, cells counted as negative for hACE2 signal
172 may express levels that are under the detection limit of the assay. Alternatively, anti-ACE2 antibodies
173 may recognize only a subpopulation of the protein by cytometry, such as, for instance, glycosylated
174 and/or truncated forms [41,42]. Of note, endogenous bACE2 expressed in NnKi cells was not
175 detectable in this assay (Fig. 2D).

176 Despite a potential underestimation of the percentage of hACE2 positive cells by flow cytometry,
177 the three assays revealed that MmBr-ACE2 and FLG-ID-ACE2 cells, both generated from brain
178 tissues, are expressing higher levels of hACE2 than the other transduced bat cell lines. Expression of
179 hACE2 and antibiotic resistance are under the control of 2 different promoters in the bicistronic
180 lentiviral vector we used. Variable strength of the two promoters in the different cell lines could
181 generate cells that survived the antibiotic treatment but express no or very little hACE2. Nevertheless,
182 despite expressing differential levels of hACE2, the hACE2-transduced cells provide models to
183 investigate the interaction between viruses belonging to the SARS-CoV-2 lineage and bat cells.

184

185 **Expression of hACE2 allows efficient replication of SARS-CoV-2 in *Myotis myotis* and**
186 ***Eptesicus serotinus* brain cells**

187 The six transduced bat cell lines and A549-ACE2 cells were infected with SARS-CoV-2 for 24
188 hours at a of MOI of 1. Cytopathic effects (CPEs) were observed in MmBr-ACE2 cells. To illustrate
189 this, we performed time-lapse microscopy of MmBr-ACE2 cells, infected or not, in the presence of
190 propidium iodide (PI) for 48 hours. Cells were rapidly forming syncytia (around 12 hours). Cell death
191 was observed as early as 34 hours, as assessed by the PI uptake through permeable cellular membranes
192 (Fig. 3A-B and movies 1 and 2). Syncytia represent cell-to-cell fusing events mediated by the
193 interaction between cell-surface expressed S proteins and ACE2 [43]. Neither CPE nor syncytia
194 formation were observed in the other cells, as illustrated by the video of infected FLG-ID-ACE2 cells
195 (Fig. 3B-C and movies 3 and 4).

196 To avoid cell death, MmBr-ACE2 cells were infected with 25 times less viruses (MOI of 0.04)
197 than the other cells (Fig. 4). Assessment of viral replication by RT-qPCR revealed that viral RNA
198 yields increased between 6 and 24 hpi in A549-ACE2 cells, and subsequently reached a plateau (Fig.
199 4A). Viral RNA yields also increased between 6 and 24 hpi in FLG-ID-ACE2 cells but then dropped
200 back to their 6h-levels (Fig. 4A), suggesting that these cells efficiently controlled viral replication.
201 Viral RNA abundance slightly increased between 6 and 24 hpi in MmNep-ACE2 cells (Fig. 4A),
202 suggesting a low level of viral RNA production, before decreasing at 48 hpi. The profile of viral RNA
203 yield was similar in MmBr-ACE2 cells and in A549-ACE2 cells (Fig. 4A), indicating a robust viral

204 replication; especially, considering that the cells were infected with 25 times less viruses than the
205 others (Fig. 4A). No increase in viral yield was observed in the 3 Nn cell lines between 6 hpi and later
206 time points (Fig. 4A), suggesting an absence of viral replication.

207 Cell lines that seemed to support viral replication (Fig. 4A), as well as one Nn cell line, were
208 analyzed for the expression of viral proteins through immunofluorescence imaging using antibodies
209 specific for S and for hACE2 at 24 hpi. Cells positive for S were observed in all cell lines (Fig 4B, C).
210 However, the proportion of positive cells varied considerably between them (Fig 4B), confirming
211 disparities in viral susceptibilities between cells of different species and/or tissues (Fig. 4A). For
212 instance, almost no cells were expressing the S protein in NnKi cells (Fig. 4B). An hACE2 signal was
213 only detected in MmBr-ACE2 cells (Fig. 4C), which are the cells that express the most hACE2 among
214 the transduced cell lines (Fig. 2B-D). Thus, as previously observed in flow cytometry assays (Fig. 2D),
215 the selected anti-hACE2 antibody appeared to allow detection in immunofluorescence analysis only
216 when the protein is expressed at high levels. The confocal images also confirmed the presence of
217 syncytia in MmBr-ACE2 infected cells (Fig. 4C). To quantify the disparities in viral protein
218 production between cells, flow cytometry analyses were performed. On average 25% of A549-ACE2
219 and MmBr-ACE2 cells were positive for S protein when infected for 24 hours at a MOI of 1 or 0.04,
220 respectively (Fig. 4D). Around 5% of FLG-ID-ACE2 and 1% of MmNep-ACE2 cells were expressing
221 the S protein (Fig. 4D). Less than 0.2% of Nn cells were positive for the S protein (Fig. 4D). These
222 flow cytometry data agree with both viral RNA yields (Fig. 4A) and e immunofluorescence analysis
223 (Fig. 4B-C). The same samples were stained with anti-hACE2 antibodies. Only around 3% of infected
224 A549-ACE2 cells appeared hACE2-positive (Fig. 4E) while around 25% of them were S-positive (Fig.
225 4D). Knowing that these cells are not permissive to viral replication in the absence of hACE2 over-
226 expression (Fig. 1A), these results further suggest that the anti-hACE2 antibodies recognized only a
227 subpopulation of ACE2. Similarly, only a fifth of FLG-ID-ACE2 cells were double-positive (Fig.
228 S2A). This under-estimation of hACE2 positive cells could also be explained by the presence of S-
229 induced syncytia (Fig. 3a and 4c), which are indeed detectable using the forward (FSC) and sideward
230 scatter (SSC) parameters of the cytometer (Fig. S2B), and likely affects the cell count. ACE2

231 expression has also been reported to be downregulated in infected human intestinal organoids [44].
232 This is also the case for infected A549-ACE2 cells (Fig. 4E).

233 Virus titration on Vero E6 cells showed that A549-ACE2 cells released around 6.10^3 PFU/ml and
234 10^4 PFU/ml at 24 and 48 hpi, respectively (Fig. 4F). Despite producing less viral RNA than A549-
235 ACE2 cells, FLG-ID-ACE2 cells yielded similar amounts of infectious particles at 24hpi (Fig. 4F).
236 Albeit not significant, less infectious particles were produced from FLG-ID-ACE2 cells at 48 hpi than
237 at 24 hpi (Fig. 4F), which is in accordance with a decrease of viral RNA production between 24 hpi
238 and 48 hpi (Fig. 4A). These data further suggest that viral replication is controlled in *E. serotinus* brain
239 cells. As expected from viral RNA and viral protein quantification (Fig. 4A and 4B), MmNep-ACE2
240 cells produced only small amounts of infectious particles, around 100 PFU/ml at 24 hpi and around 60
241 PFU/ml at 48 hpi (Fig. 4F). MmBr-ACE2 cells released only around 10 PFU/ml, which is 1000 times
242 less than A549-ACE2 cells (Fig. 4F). This was surprising since the two cell lines produced similar
243 quantities of viral RNAs and proteins (Fig. 4A-D). Approximately 100 PFU/ml were collected from
244 the supernatant of the three lines of Nn cells, a similar amount to what was detected in non-permissive
245 cells, such as non-transduced A549, FLG-ID and Nnki cells, which were included in the analysis as
246 negative controls (Fig. 4F). These infectious particles are thus likely input viruses that were carried
247 over from the inoculum of the first round of infection.

248 Together, these data revealed that expression of hACE2 allowed the virus to complete its
249 replication cycle in *E. serotinus* FLG-ID brain cells, suggesting an ACE2-mediated refractory state to
250 SARS-CoV-2 replication. Expression of hACE2 in *M. myotis* brain cells (MmBr-ACE2) allows the
251 production of viral RNA and proteins, indicating that the ACE2-mediated restriction can also be
252 overcome. However, infectious particles were not released from these cells, suggesting the existence
253 of another cellular restriction at a later stage of the viral replication cycle. In MmNep-ACE2 and Nn
254 cells, expression of hACE2 was not sufficient to allow robust viral replication, suggesting a deficiency
255 in key proviral factor(s) and/or expression of potent antiviral factor(s).

256

257 **Infectious particles are produced by MmBr-ACE2 cells but are not released**

258 Since MmBr-ACE2 cells sustained the production of viral RNAs and proteins (Fig. 4A-C-D), we
259 were intrigued by the absence of infectious particles release (Fig. 4F). Despite infecting these cells
260 with a MOI of 0.04 (Fig. 4) to reduce the CPEs observed at a MOI of 1 (Fig. 3), we wondered whether
261 cytokines released by infected cells and/or dying cells may stimulate damage-associated molecular
262 patterns (DAMPs) and thus trigger an antiviral response inhibiting viral replication in Vero E6 cells.
263 Other possibilities include a defect in viral assembly and/or in viral transport through the secretory
264 pathway in MmBr-ACE2 cells. Alternatively, these cells may only produce immature non-infectious
265 viral particles. To investigate these hypotheses, supernatants collected from MmBr-ACE2 cells, and as
266 controls, from A549-ACE2 and MmNep-ACE2 cells, were clarified by ultracentrifugation to get rid of
267 potential cytokines and cell debris and titrated on Vero E6 cells. Flow cytometry analysis using anti-S
268 antibodies were done on the same samples to verify that the cells were infected (Fig. 5A). Clarified
269 and ultracentrifuged supernatants from A549-ACE2 and MmNep-ACE2 cells contained similar
270 amounts of infectious particles, around 10^4 PFU/ml and 100 PFU/ml, respectively (Fig. 5B).
271 Comparable to observations in previous experiments (Fig. 4F), little infectious particles, around 10
272 PFU/ml, were recovered in both the clarified and ultracentrifuged supernatant of infected MmBr-
273 ACE2 cells (Fig. 5B). These data suggest that immunostimulatory components, such as cytokines or
274 dying cells, that could be present in infected MmBr-ACE2 cell culture supernatants did not affect the
275 results of the titration assays. To assess the presence of intracellular infectious particles in MmBr-
276 ACE2 cells, the titration assays were performed on crude cell lysates collected at 24 hpi. Around one
277 log more infectious particles were retrieved from lysed A549-ACE2 cells than from their supernatant
278 (Fig. 5B). By contrast, only 10^2 PFU/ml viral particles were collected in lysed MmNep-ACE2 cells
279 (Fig. 5B). These results agree with the level of viral replication previously detected in A549-ACE2
280 and MmNep-ACE2 cells (Fig. 4). Around 3 log more viral particles (about 10^4 PFU/ml) were retrieved
281 from lysed MmBr-ACE2 cells than in the culture supernatant (Fig. 5B), suggesting that viral assembly
282 and maturation takes place in these cells and that the absence of viral release is likely due to a defect in
283 viral transport through the secretory pathway. Thus, MmBr-ACE2 cells are either missing one or
284 several cellular factor(s) that are required for exit of infectious virions from assembly sites to the cell
285 membrane and/or they express one or several antiviral factor(s) that potently block this transport.

286

287 **An abortive entry route exists in bat and human cells**

288 To investigate further ACE2-mediated restriction, we performed binding and entry assays on cells
289 transduced or not with hACE2 (Fig. 6A). Infected cells were kept on ice for 1 hour, washed three
290 times and then either lysed ('on ice') or incubated at 37 degrees for 2 or 6 hours. To remove potential
291 residual bound particles, the warmed cells were treated with trypsin for 30 minutes prior to lysis. We
292 performed the assays with A549, FLG and NnKi cells since they tolerated the three washes on ice
293 without detaching from the plates and, for each cell line, we compared viral RNA abundance in wild-
294 type *versus* hACE2-expressing cells. Viral RNA detected in cells that were kept on ice represent input
295 viruses bound to cellular membranes. In all six cell lines, we indeed detected viral RNA bound to cell
296 membranes (Fig. 6A), suggesting that hACE2 expression is not required for viral attachment. Such
297 ACE2-independent binding of the S protein could be mediated by heparan sulfate, as described for
298 several human cell lines [45,46], or by endogenous ACE2 when it is expressed at detectable levels
299 (Fig. 2A). hACE2 expression may however enhance viral binding to the A549 and FLG cell
300 membranes since around 500 more genome copies per μg of total RNA were detected in cold
301 transduced cells than in unmodified ones (Fig. 6A). Abundance of viral RNAs increased between 2
302 and 6 hours both in A549-ACE2 and FLG-ACE2 cells but not in wild-type cells (Fig. 6A). These
303 results confirm that viral replication occurred hACE-2 expressing A549 and FLG cells (Fig. 4). No
304 increase in viral RNA yield was observed between 2 and 6 hours in NnKi-ACE2 cells (Fig. 6A),
305 confirming the absence of viral replication in these cells (Fig. 4). Viral RNA detected at 2 or 6 hpi in
306 non-transduced cells (Fig. 6A) may represent viruses that remained attached to the cell surface despite
307 the trypsin treatment or viruses that penetrated the cells via an hACE2-independent route. To ensure
308 that the trypsin treatment was effective in cleaving off particles bound to the cell surface, A549 and
309 NnKi cells kept on ice for one hour were treated with trypsin for 30 minutes (Fig. 6B). Around 2 to 3
310 log less viral RNA was detected in trypsinized A549 and NnKi cells than in non-treated cells (Fig.
311 6B), suggesting that a large quantity of viruses is indeed detaching from cell membranes upon trypsin
312 treatment. Significantly more viral RNA was detected in A549 and NnKi cells that had been shifted to
313 37 degrees for 2 h than in iced cells treated with trypsin (Fig. 6B). These viral RNA molecules may

314 represent virions that penetrated the cells. Together, these data suggest that viruses are internalized in
315 cells that do not over-express ACE2 (Fig. 6). This internalization path does not, however, lead to a
316 productive viral cycle (Fig. 1 and 4).

317

318 **Viral IFN counteraction mechanisms are species-specific**

319 Quantification of intracellular viral RNAs and titration assays revealed that FLG-ACE2 cells,
320 and, to a lesser extent, MmNep-ACE2 cells, controlled viral replication over time (Fig. 4A and D). By
321 contrast, viral RNA yield remained high between 24 and 48 hpi in A549-ACE2 and MmBr-ACE2
322 cells (Fig. 4A and D). To assess whether the interferon (IFN) response could contribute to viral
323 containment in FLG-ACE2 and MmNep-ACE2 cells, we compared mRNA abundance of two IFN-
324 stimulated genes (ISGs) upon stimulation or infection in the different cell lines. We selected OAS1
325 and IFIH1, 2 ISGs that are conserved across vertebrate species [47]. Moreover, OAS1 expression is
326 associated with reduced COVID-19 death [48] and IFIH1 codes for Mda5, the protein responsible for
327 sensing SARS-CoV-2 replication intermediates, and thus initiating the IFN response, in human
328 cells[49,50]. We first evaluated the expression of the two selected ISGs upon transfection with
329 polyI:C, a synthetic dsRNA analog. All seven cell lines contained transcripts for these two ISGs and
330 responded well to the stimulation (Fig. 7A-B), demonstrating that they possess intact IFN- induction
331 and -signaling pathways.

332 We then evaluated the mRNA abundance of these two ISGs in cells infected for 6, 24 and 48
333 hours (Fig. 7C-D). No increase of OAS1 and IFIH1 expression was observed in A549-ACE2 cells
334 (Fig. 7C-D). This agrees with a previous report showing that infection of A549-ACE2 by SARS-CoV-
335 2 is characterized by an absence of IFN response [51]. By contrast, the abundance of OAS1 and IFIH1
336 transcripts increased between 6 and 24 hpi in FLG-ACE2 and MmNep-ACE2 cells (Fig. 7C-D) and
337 remained elevated at 48 hpi in both cell lines (Fig. 7C-D). In MmBr-ACE2 cells, the infection
338 triggered the induction of OAS1 expression but not of IFIH1 (Fig. 7C-D), suggesting that the virus is
339 able to suppress IFN-mediated Mda5 upregulation in this cell type. No or little stimulation of OAS1
340 and IFIH1 expression was observed in Nn cells upon viral infection (Fig. 7C-D). This was expected
341 since the virus replicates at very low levels in these cells (Fig. 4). Surprisingly, the mRNA abundances

342 of both OAS1 and IFIH1 were lower in NnLi-ACE2 cells exposed to the virus for 6 h than in control
343 cells (Fig. 7C-D). Such downregulation was also observed for IFIH1 in NnKi-ACE2 cells. Since only
344 around 0.1% of Nn cells are producing S proteins (Fig. 4D), this decrease in OAS1 and IFIH1
345 expression is replication-independent. It could be mediated by innate immune sensors present at the
346 cell surface and/or in endosomal compartments, where the virus may be retained (Fig. 6), such as toll-
347 like receptors (TLRs) [52].

348 Together, our data confirmed that SARS-CoV-2 efficiently counteracts ISG induction in A549-
349 ACE2 cells [51] and revealed that it is not the case in FLG-ACE2 and MnNep-ACE2 cells. The
350 control of viral replication observed in these two cell lines (Fig. 4) could thus be due to the expression
351 of a set of ISGs with potent antiviral functions. Interestingly, IFN-mediated barriers are not only
352 species-specific but also organ-specific since the virus dampens Mda5 expression in MmBr-ACE2
353 cells but not in MmNep-ACE2 cells.

354

355 Discussion

356 The development of novel bat cellular models is essential to understand the molecular
357 mechanisms underlying the ability of bats to serve as reservoirs for numerous viruses, including alpha-
358 and beta-coronaviruses. We first produced *R. ferrumequinum*, *M. myotis*, *M. nattereri* and *M. brandtii*
359 primary cells to evaluate their susceptibility to infection with the initial SARS-CoV-2. None of them
360 supported viral replication, not even *R. ferrumequinum*, which belongs to the same genus as the host
361 (*R. affinis*) of RaTG13, a potential ancestor of SARS-CoV-2 [4]. These primary cells, which were
362 generated from patagium biopsies of living bats, exhibited a dermal-fibroblast phenotype. A single-
363 cell transcriptomic analysis showed that *R. sinicus* skin cells express moderate levels of ACE2 and
364 very little TMPRSS2 [53]. The virus may thus be able to enter the skin primary cells that we generated
365 but the fusion step could be the factor limiting infection. Further experiments will be required to
366 characterize at which step of its replicative cycle the virus is stopped in these primary cells.

367 We established the first three *Nyctalus noctula* cell lines using liver, kidney and lung tissues from
368 a single bat. These organs are site of viral replication in infected patients [37] and may thus be
369 physiologically relevant for bat infection as well. Similar to the cells originated from *M. myotis* and *E.*

370 *serotinus* bat species, all three Nn cell lines responded well to stimulation with synthetic dsRNA,
371 indicating that they are valuable tools to study the bat innate immune response. In addition to
372 coronaviruses, *N. noctula* carries other viruses with zoonotic potential such as paramyxoviruses and
373 hantaviruses [54,55]. The Nn cells that we have developed represent thus novel opportunities to study
374 bat-borne viruses. We found that Nn kidney cells expressed higher levels of ACE2 than Nn cells
375 derived from lung or liver. Likewise, ACE2 is expressed at high levels in *R. sinicus* kidney, as
376 revealed by comparative single-cell transcriptomic [53] and *in silico* [56] analysis of ACE2 expression
377 pattern in various tissues. ACE2 is also highly expressed in human kidney [57]. Thus, kidney cells
378 appear relevant to study betacoronavirus replication. Finally, we have generated six bat cell lines
379 expressing hACE2. The varying susceptibilities of the six transduced cells to SARS-CoV-2 infection
380 offer opportunities to decipher species-specific antiviral mechanisms that have evolved in bats. A
381 obvious need to develop additional bat cell lines still remains [30]. Particularly valuable cells would be
382 cells derived from bat intestine, a tissue that expresses high level of proteins known to mediate or
383 facilitate cellular entry of bat-borne betacoronaviruses, such as ACE2 and TMPRSS2, at least in *R.*
384 *sinicus* [53], and that is relevant for SARS-CoV-2 infection, as demonstrated by the detection of viral
385 genomes in duodenum tissue of experimentally infected *Rousettus aegypticus* [29].

386 *Myotis myotis*, *Tadarida brasiliensis*, *Eptesicus serotinus*, and *Nyctalus noctula* cells were
387 resistant to infection with both the initial virus and two recently emerged variants. ACE2 from *M.*
388 *myotis* and *T. brasiliensis*, as well as from a species of the *Eptesicus* genus, permitted S-mediated
389 entry of pseudotyped VSV when ectopically expressed in human cells refractory to SARS-CoV2
390 infection [22]. This means that when expressed at high levels, ACE2 from these three species interacts
391 with the viral S protein. As in human A549 cells, ACE2 may be expressed at a level which is too low
392 to allow viral entry in our bat cell line models. Potential ability of *N. noctula* ACE2 to bind S protein
393 has not been reported and the genome of this bat genus is yet to be sequenced. Hence, low affinity
394 between S protein and ACE2 and/or low level of ACE2 expression may hamper viral replication in
395 these cells. Our results highlight the importance of performing experiments in the context of genuine
396 infection of bat cells to predict their susceptibility to infection.

397 Trypsin-resistant viruses were detected in non-transduced A549, FLG-ID and NnKi cells at early
398 time post-infection. They likely represent input viruses that penetrated the cells despite the absence of
399 hACE2 expression. These viruses could have entered cells using bACE2 or via an ACE2-independent
400 manner. Such ACE2-independent entry has been described previously in Vero E6 cells [19]. By
401 contrast to what is observed in Vero E6 cells, these two potential paths are abortive in A549, FLG-ID
402 and NnKi cells since it doesn't allow viral replication. The virus may be routed to a subset of
403 endosomes that lack appropriate proteases. Expression of hACE2 allowed efficient viral RNA and
404 protein production in A549, FLG-ID and Mm cells, suggesting that these cells express proteases that
405 efficiently cleave S proteins. It also shows that ACE2 alone was responsible for the lack of viral
406 replication in non-transduced A549, FLG-ID and Mm cells. This ACE2-mediated entry block is rather
407 due to a low or absent ACE2 expression than to an incompatibility between ACE2 and S protein since
408 ectopic expression of *Myotis* spp. and *Eptesicus* spp. ACE2 facilitate S-mediated entry of pseudo-
409 viruses [22,23]. By contrast, expressing hACE2 in Nn cells, at a higher level than in permissive Caco-
410 TC7 cells, seems sufficient to permit internalization but not replication. Nn cells may not express
411 proteases able to cleave S protein and virions are thus probably retained in endosomes.

412 Infectious particles were produced in Mm cells but were not released into the extracellular milieu.
413 Instead of using the canonical secretory pathway exploited by many enveloped viruses to exit cells,
414 betacoronaviruses hijack lysosomes for their transport from assembly sites to the plasma membrane
415 [58]. Mm cells maybe deficient in one or several components of this lysosomal pathway. Since
416 infection induced S-mediated syncytia formation in Mm cells, viruses might spread from cell-to-cell
417 via syncytia, as do other syncytia-forming viruses such as respiratory syncytial virus, parainfluenza
418 viruses and measles[59]. Syncytia-mediated intercellular spreading allows viruses to escape virus-
419 neutralizing antibodies. Such mode of transport has been previously proposed in human cells infected
420 with the Middle East Respiratory Syndrome coronavirus (MERS-CoV) [60], another betacoronavirus.
421 Analysis of *post-mortem* samples of patients that succumb of COVID-19 revealed the presence of
422 syncytial pneumocytes positives for viral RNAs [61]. However, the pathogenetic significance of
423 syncytia remains to be investigated.

424 SARS-CoV-2 has evolved numerous synergetic mechanisms to evade the IFN response in human
425 cells [62], resulting in an absence of IFN expression in some cells, including A549 cells [51,63]. The
426 virus is unable to counteract ISG induction in *Eptesicus serotinus* kidney cells and in *Myotis myotis*
427 nasal epithelial cells. This is especially intriguing in *E. serotinus* cells since the virus replicates to high
428 levels in these cells and thus produce proteins with described IFN antagonist activities. Similarly,
429 MERS-CoV suppresses the antiviral IFN response in human cells but not in *E. fuscus* cells [64]. One
430 can envisage that escape of IFN-mediated restriction by betacoronaviruses is species-specific. For
431 instance, SARS-CoV-2 Nsp14 targets human IFNAR1 for lysosomal degradation [62], but may be
432 unable to degrade bat IFNAR1. This inability to evade IFN response in *Eptesicus serotinus* kidney
433 cells and in *Myotis myotis* nasal epithelial cells may contribute to the cellular control of infection in
434 FLG-ID and MmNep cells, as in experimentally infected *Eptesicus fuscus* [65]. Other mechanisms
435 could be at play. For instance, the basal level of IFN may be high in these two cell lines, as reported in
436 several other bat species[66–68]. Expression of a mutated form of IRF3, which is a key transcription
437 factor involved in the induction of the IFN signaling cascade, contributes to an enhanced IFN response
438 in bat species, including in *E. fuscus*, as compare to human [69]. Investigation of IRF7, another
439 transcription factor that mediates IFN expression, in *Pteropus alecto* cells revealed a more widespread
440 tissue distribution in bats than in humans [70,71]. Bats may thus launch IFN-dependent measures
441 against viruses in a faster and broader manner than in humans [72]. Another possibility to explain the
442 high level of ISG expression in infected *E. serotinus* kidney cells is that they express specific set of
443 potent antiviral ISGs. Expression of atypical ISGs has been reported for different bat species,
444 including RNA-degrading ribonuclease L (RNaseL) in *P. alecto* cells and RNA-binding Microorchidia
445 3 (MORC3) in *Pteropus vampyrus* and *Eidolon helvum* cells [66,73]. Pursuing the characterization of
446 bat innate immunity in relevant *in vitro* models is essential to understand the mechanisms by which
447 they control the replication of numerous unrelated viruses.

448

449 **Materials and Methods**

450 **Bat primary cells.** *M. myotis* samples were collected in July 2020 from two bat colonies in Inca
451 and Lluçmajor on Mallorca (Balearic Islands, Spain) (agreement CEP 31/2020 delivered by the

452 Ministry of the Environment and Territory, government of the Balearic Islands). *R. ferrumequinum*
453 biopsies were collected in France in 2020. Authorization for bat capture was delivered by the French
454 Ministry of Ecology, Environment and Sustainable development (approval C692660703 from the
455 Departmental Direction of Population Protection (DDPP), Rhone, France). All methods were approved
456 by the ‘Muséum National d’Histoire Naturelle (MNHN)’ and the ‘Société Française pour l’Étude et la
457 Protection des Mammifères (SFEPM)’. Patagium biopsies were shipped in freezing medium Cryo-
458 SFM (PromoCell), on dry ice or at 4°C with ice packs. Primary cells were obtained as previously
459 described [74,75]. Briefly, skin biopsies were washed twice with sterile PBS, excised in small pieces
460 and enzymatically digested, either with 500 µL of collagenase D (1 mg/mL) (Roche) and overnight
461 incubation at 37°C without agitation, or with 100-200 µL of TrypLE Express Enzyme (Gibco) and
462 incubation 10 min at 37°C under gentle agitation. Dissociated cells and remaining pieces of tissue
463 were placed in a single well of a 6-well plate containing 2 mL of Dulbecco's Modified Eagle Medium
464 (DMEM, Gibco) containing 20% heat-inactivated fetal bovine serum (FBS) (Eurobio), 1%
465 penicillin/streptomycin (P/S) (Gibco), and 50 µg/ mL gentamycin (Gibco), and incubated at 37°C
466 under 5% CO₂. Cell cultures were regularly checked to determine the need for media refreshment or
467 splitting. After 5-10 passages, cells were grown in DMEM supplemented with 10% FBS.

468

469 **Cell lines.** FLG-ID, FLG-R, FLN-ID, FLN-R and Tb1Lu cell lines (table 1) were maintained in
470 equal volumes of Ham’s F12 and Iscove’s modified Dulbecco’s medium (IMDM, Gibco),
471 supplemented with 10% FBS and 1% P/S (Gibco) in non-vented flasks. Mm cells, which were
472 obtained from a single common serotine bat (*Eptesicus serotinus*), were previously described [36]. Nn
473 kidney-, liver- and lung-derived cell cultures were obtained from a common noctule bat (*Nyctalus*
474 *noctula*) euthanized because of poor chance of survival associated with traumatic injuries sustained
475 while a dead tree sheltering bat hibernaculum was cut. The decision to euthanize the specimen was
476 made by a veterinarian following inspection of a group of noctule bats presented for examination and
477 therapy in the rescue center at the University of Veterinary and Pharmaceutical Sciences Brno, Czech
478 Republic, in November 2015 [76]. The bat was anesthetized with isofluranum (Piramal Enterprises
479 Ltd.) and euthanized by quick decapitation. The cadaver was immersed into 96% ethanol for a few

480 seconds and then subjected to necropsy under aseptic conditions to collect organs which were
481 loosened mechanically with scalpel blades, minced into small pieces, suspended in DMEM (Biosera)
482 containing 1 mg/ml collagenase (Thermo Fisher Scientific) and 1 mg/ml trypsin (Sigma-Aldrich), and
483 incubated at 37 °C on a shaking thermoblock for 45 min. The cells were then separated through a 100
484 µm nylon filter and washed twice in a medium supplemented with 10% FBS to stop enzymatic
485 digestion. The cells yielded in this way were cultured in DMEM supplemented with 10% FBS and 1%
486 P/S (Sigma). Primary cells were immortalized by transfection of pRSVAg1 plasmid expressing Simian
487 Vacuolating Virus 40 large T antigen (SV40T) with lipofectamine 2000 (Invitrogen) according to the
488 manufacturer's protocol, expanded and cryopreserved. Mm and Nn cell lines (table 1), as well as
489 African green monkey Vero E6 cells (ATCC CRL-1586), human lung epithelial A549 cells (kind gift
490 from Frédéric Tangy, Institut Pasteur, Paris) and human colorectal adenocarcinoma Caco TC7 cells
491 (ATCC HTB-37), were maintained in DMEM (Gibco), supplemented with 10% FBS and 1% P/S in
492 vented flasks. All cells were maintained at 37°C in a humidified atmosphere with 5% CO₂. Bat and
493 A549 cells were modified to stably express hACE2 using the pLenti6-hACE2 lentiviral transduction
494 as described previously [43]. Briefly, 2x10⁵ cells were resuspended in 150 µl of culture medium
495 containing 15 µl of ultracentrifuged lentiviral vectors supplemented with 2mM HEPES (Gibco) and 4
496 µg/ml polybrene (Sigma). Cells were agitated for 30 sec every 5 min for 2.5 h at 37°C in a
497 Thermomixer and then plated. 48 h after transduction, blasticidin (concentrations ranging from 7-15
498 µg/ml depending on cell lines) was added in the culture media.

499

500 **Virus and infections.** The SARS-CoV-2 strain BetaCoV/France/IDF0372/2020 (historical) and
501 hCoV-19/France/PDL-IPP01065/2021 (20H/501Y.V2 or SA) were supplied by the French National
502 Reference Centre for Respiratory Viruses hosted by Institut Pasteur (Paris, France) and headed by Pr.
503 S. van der Werf. The human samples from which the historical and South African strains were isolated
504 were provided by Dr. X. Lescure and Pr. Y. Yazdanpanah from the Bichat Hospital, Paris, France and
505 Dr. Vincent Foissaud, HIA Percy, Clamart, France, respectively. These strains were supplied through
506 the European Virus Archive goes Global (EVAg) platform, a project that has received funding from
507 the European Union's Horizon 2020 research and innovation program under grant agreement

508 #653316. The hCoV-19/Japan/TY7-501/2021 strain (20J/501Y.V3 or Brazil) was kindly provided by
509 Jessica Vanhomwegen (Environment and Infectious Risks Research and Expertise Unit; Institut
510 Pasteur). Viral stocks were produced by amplification on Vero E6 cells, for 72 h in DMEM
511 supplemented with 2% FBS and 1% P/S. The cleared supernatant was stored at -80°C and titrated on
512 Vero E6 cells by using standard plaque assays to measure plaque-forming units per mL (PFU/mL).
513 Cells were infected at the indicated multiplicities of infection (MOI) in DMEM without FBS. Virus
514 inoculum was either removed after 6 h and replaced or topped up with FBS containing culture medium
515 to a final concentration of 2% FBS and 1% P/S. For infections with proteolytically activated SARS-
516 CoV-2, cell monolayers were washed twice with PBS before adding virus inoculum in DMEM
517 supplemented with 1µg/ml of trypsin TPCK (Sigma) and no FBS. After 4h, DEMEM containing FBS
518 was added to a final concentration of 2%.

519 **TCID₅₀ assays.** Supernatants of infected cells were 10-fold serially diluted in DMEM
520 supplemented with 2% FBS and 1% P/S. To remove cytokines and other proteins, supernatants were
521 ultracentrifuged for 1 h at 45k rpm at 4°C and resuspended in DMEM with 2% FBS and 1% P/S after
522 4 h incubation at 4°C. Infected cells were lysed and scraped in ddH₂O. After one freeze-thaw cycle,
523 whole cell lysates were cleared by centrifugation, supplemented with 10x PBS to a physiological
524 condition and used for serial dilutions. Around 9x10³ Vero E6 cells and 50 µl of serially diluted virus
525 suspensions were deposited in 96-well plate in quintuplicate wells. Cells were fixed with 4%
526 paraformaldehyde (PFA) for 30 min at RT and revealed with crystal violet 5 days later. Cytopathic
527 effects (CPE) were assessed by calculating the 50% tissue culture infective dose (TCID₅₀) using the
528 Spearman-Kärber method [77].

529 **Flow cytometry.** Cells were detached with trypsin or versene for hACE2 staining. Cells were
530 then fixed in 4% PFA for 30 min at 4°C and staining was performed in PBS, 2% BSA, 2mM EDTA
531 and 0.1% Saponin (FACS buffer). Cells were incubated with goat pAB anti-hACE2-647 (1:100,
532 FAB933R R&D Systems) and/or with antibodies recognizing the spike protein of SARS-CoV (anti-S,
533 1:1000, GTX632604 Genetex) or anti-S mAb10 (1 µg/ml, a kind gift from Dr. Hugo Mouquet, Institut
534 Pasteur, Paris, France) and subsequently with secondary antibodies anti-human AlexaFluor-647

535 (1:1000, A21455 Thermo), anti-mouse AlexaFluor-488 (1:1000, A28175 Thermo) or Dylight488
536 (1:100, SA5-10166 Thermo) for 30 min at 4°C. Cells were acquired on an Attune NxT Flow
537 Cytometer (Thermo Fisher) and data analyzed with FlowJo software v10 (TriStar).

538 **RNA extraction and RT-qPCR assays.** Total RNA was extracted from cells with the
539 NucleoSpin RNA II kit (Macherey-Nagel) according to the manufacturer's instructions. First-strand
540 complementary DNA (cDNA) synthesis was performed with the RevertAid H Minus M-MuLV
541 Reverse Transcriptase (Thermo Fisher Scientific) using random primers. For batACE2 determination,
542 total RNA was treated with DNase I (DNase-free kit, Thermo Fisher Scientific) for 30 min at 37°C
543 before cDNA synthesis with SuperScript IV reverse transcriptase. Quantitative real-time PCR was
544 performed on a real-time PCR system (QuantStudio 6 Flex, Applied Biosystems) with Power SYBR
545 Green RNA-to-CT 1-Step Kit (Thermo Fisher Scientific). Data were analyzed using the $2^{-\Delta\Delta CT}$
546 method, with all samples normalized to GAPDH. Genome equivalent concentrations were determined
547 by extrapolation from a standard curve generated from serial dilutions of the pcDNA3.1-hACE2
548 plasmid (addgene, 145033) or plasmids encoding a fragment of the RNA-dependent RNA polymerase
549 (RdRp)-IP4 of SARS-CoV-2 or a fragment of the ACE2 genome of each bat species. Primers used for
550 RT-qPCR analysis are given in table S1.

551

552 **Cloning of qPCR amplicon.** To quantify the amounts of bat ACE2 in each cell line, plasmids
553 containing the qPCR amplicon obtained with the primers described in table S1 were generated via
554 TOPO cloning. Briefly, total RNA was extracted from a cadaver of *Myotis myotis* stored at the
555 University of Veterinary and Pharmaceutical Sciences in Brno. For the remaining two bat species,
556 total RNA extracted from NnKi and FLG-R cells were used. RNA was treated for 30 min at 37°C with
557 DNase I and cDNA synthesized with SuperScript IV reverse transcriptase. These cDNAs were then
558 used as template for PCR amplification of the qPCR bACE2 amplicon using the primers in table S1
559 and Phusion High-fidelity DNA Polymerase (Thermo). PCR products were gel-purified (NucleoSpin
560 gel and PCR clean-up kit, Macherey-Nagel) and cloned into pCR-Blunt II-TOPO vectors using the

561 Zero Blunt TOPO PCR Cloning Kit (Thermo). Inserts were verified via Sanger sequencing. Plasmids
562 were then used as quantitative qPCR standards.

563

564 **Western blot analysis.** Proteins extracted from cell lysates were resolved by SDS-
565 polyacrylamide gel electrophoresis on 4-12% NuPAGE Bis-Tris Gel (Life Technologies) with MOPS
566 running buffer and semi-dry transferred to a nitrocellulose membrane with Trans-Blot Turbo system
567 (Bio-Rad). After blocking with 0.05% Tween20 in PBS (PBST) containing 5% dry milk powder for 1
568 h at room temperature (RT), the membrane was incubated with goat pAB anti-hACE2-700 (1:200,
569 FAB933N R&D Systems) and mouse mAB anti-b-actin (1:5000, A5316 Sigma) diluted in blocking
570 buffer overnight at 4°C. The membranes were then incubated with DyLight800 secondary AB
571 (1:5000, 46421 Thermo) diluted in blocking buffer for 1 h. Finally, the membranes were revealed
572 using an Odyssey CLx infrared imaging system (LI-COR Bioscience).

573 **Immunofluorescence microscopy and live cell imaging.** Cells grown on glass coverslips were
574 fixed in 4% PFA for 30 min at RT and permeabilized with 0.2% Triton X-100 (Sigma/Merck) in PBS
575 for 10 min at RT. Following blocking with 3% bovine serum albumin (BSA, Sigma) in PBS for 1 h at
576 RT, cells were incubated with goat pAB anti-hACE2 (1:50, AF933 R&D Systems) and mAB anti-
577 SARS-CoV-2-spike (1:1000, GTX632604 Genetex) in 1% BSA in PBS (AB buffer) for 1h at RT or
578 overnight at 4°C. Subsequently, cells were incubated with anti-goat Alexa488 (A-11055, Thermo
579 Fisher Scientific) and anti-mouse Alexa555 (A21427, Thermo Fisher Scientific) secondary antibodies
580 diluted 1:500 in AB buffer for 30 min at RT. Finally, cells were stained with NucBlue Fixed Cell
581 ReadyProbes reagent (Thermo) in PBS for 5 min at RT. Coverslips were washed with ultrapure water
582 (Gibco) and mounted in ProLong Gold antifade (Life Technologies). Sample were visualized with a
583 Leica TCS SP8 confocal microscope (Leica Microsystems) and a white light excitation laser and a
584 405nm diode laser were used for excitation. Confocal images were taken with automatically optimized
585 pixel format, a 4× frame averaging and a scan speed of 400 Hz through an HC PL APO CS2 63x NA
586 1.4 oil immersion objective. Overlay pictures of single channel images were digitally processed in
587 Leica LAS X lite software. For live imaging, 5.4×10^4 to 10^5 cells were plated per quadrant in a μ -Dish

588 35 mm Quad dish (80416, Ibidi). Cells were infected the next day with SARS-CoV-2 at a MOI of 1 in
589 culture media supplemented with 2.5% FBS and 1% P/S containing propidium iodide. Transmission
590 and fluorescence images were taken at 37°C every 15 min, up to 48 h, using a Nikon BioStation IMQ,
591 with three fields for each condition.

592 **Attachment and entry assays.** Cells plated in monolayers were pre-chilled on ice for 10 min and
593 washed once with cold PBS. Cells were then incubated with SARS-CoV-2 at a MOI of 1 for 1 h on
594 ice. Following three washes with cold PBS, half of the cells was lysed in RA1 lysis buffer (Macherey-
595 Nagel) (“on ice”). The second half of the cells was trypsinized for 15 min on ice and 15min at 37°C
596 after washing of the virus inoculum, then washed with PBS and lysed (“on ice + trypsin”). The
597 remaining cells were directly transferred to 37°C after washing of the virus inoculum and incubated
598 for 2 or 6 h in warm culture media supplemented with 2% FBS and 1% P/S. After this incubation
599 period, those cells were trypsinized for 30 min at 37°C, washed with PBS and lysed in RA1 buffer
600 (“2h”, “6h”). Finally, total RNA was extracted from all cell lysates using the NucleoSpin RNA II kit
601 (Macherey-Nagel).

602 **PolyI:C stimulation.** Cells were plated in monolayers in 24-well culture plates. The next day,
603 they were transfected with 250 ng low molecular weight Poly I:C (InvivoGen) or PBS, respectively,
604 using INTERFERin (Polyplus transfection) transfection reagent. Cells were lysed 16 h after
605 transfection and total RNA was extracted using the NucleoSpin RNA II kit (Macherey-Nagel).

606 **Statistical analysis.** Graphical representation and statistical analyses were performed using
607 GraphPad Prism Version 9.0.2 software (GraphPad). Unless otherwise stated, results are shown as
608 means \pm SD from 3 independent experiments. Significance was calculated using either Dunnett’s
609 multiple comparison test on a two-way ANOVA analysis or Šídák’s multiple comparisons test on a
610 two-way ANOVA analysis as indicated. Statistically significant differences are indicated as
611 follows: * $p < 0.05$; ** $p < 0.01$; *** $p < 0.001$; **** $p < 0.0001$; and ns, not significant.

612 **Acknowledgments.** We thank Noémie Aurine (Université Lyon 1, France) for her help designing
613 RT-qPCR primers for bat samples; Bertrand Pain (Université Lyon 1, France) for his advices in both
614 bat primers design and generation of bat primary cell lines; Ondine Filippi-Codaccioni and Marc
615 López-Roig (Université Lyon 1, France) for their precious help in bat sampling; the French National
616 Reference Centre for Respiratory Viruses hosted by Institut Pasteur (France) and headed by Pr. S. van
617 der Werf for providing the historical viral strains and the SA variant; Jessica Vanhomwegen (Institut
618 Pasteur, France) for providing the Brazilian variant; Hugo Mouquet and Cyril Planchais (Institut
619 Pasteur, France) for providing anti-S antibodies; Françoise Porrot for lentiviral production (Institut
620 Pasteur, France); Florence Guivel-Benhassine (Institut Pasteur, France) for help in titration assays;
621 Thomas Vallet (Institut Pasteur, France) for help performing experiments with the viral variants and
622 Matthias Lenk (Friedrich-Loeffler-Institut, Germany) for providing the *E. serotinus* cell lines. We are
623 grateful to the members of our laboratories for helpful discussions. We acknowledge the UTechS
624 Photonic BioImaging (Imagopole), C2RT, Institut Pasteur, supported by the French National Research
625 Agency (France BioImaging; ANR-10-INBS-04; Investments for the Future) for the use of the
626 confocal microscope.

627

628 **Funding.** This work was funded by the CNRS (NJ, OS), Institut Pasteur (NJ, LD, OS), ‘Urgence
629 COVID-19’ fundraising campaign of Institut Pasteur (NJ, LD, OS), the University of Veterinary
630 Sciences of Brno (FVHE/Pikula/ITA2021) (JP), LabEx Ecofect (ANR-11-LABX-0048) (DoP), Labex
631 IBEID (ANR-10-LABX-62-IBEID) (OS), ANR/FRM Flash Covid PROTEO-SARS-CoV-2 (OS) and
632 IDISCOVER (OS). S.M.A. and De.P. are supported by the Pasteur-Paris University (PPU) International
633 PhD Program and the Vaccine Research Institute (ANR-10-LABX-77), respectively. D.S.L. was
634 funded by the Chinese Scholarship Council and Institut Pasteur. The funders had no role in study
635 design, data collection and analysis, decision to publish, or preparation of the manuscript.

636

637 **References**

- 638 1. Zhou H, Chen X, Hu T, Li J, Song H, Liu Y, et al. A Novel Bat Coronavirus Closely Related to
639 SARS-CoV-2 Contains Natural Insertions at the S1/S2 Cleavage Site of the Spike Protein.
640 *Current Biology*. 2020;30: 2196-2203.e3. doi:10.1016/j.cub.2020.05.023
- 641 2. Yang X-L, Hu B, Wang B, Wang M-N, Zhang Q, Zhang W, et al. Isolation and Characterization
642 of a Novel Bat Coronavirus Closely Related to the Direct Progenitor of Severe Acute
643 Respiratory Syndrome Coronavirus. Perlman S, editor. *J Virol*. 2016;90: 3253–3256.
644 doi:10.1128/JVI.02582-15
- 645 3. Boni MF, Lemey P, Jiang X, Lam TT-Y, Perry BW, Castoe TA, et al. Evolutionary origins of
646 the SARS-CoV-2 sarbecovirus lineage responsible for the COVID-19 pandemic. *Nature*
647 *Microbiology*. 2020; 1–10. doi:10.1038/s41564-020-0771-4
- 648 4. Zhou P, Yang X-L, Wang X-G, Hu B, Zhang L, Zhang W, et al. A pneumonia outbreak
649 associated with a new coronavirus of probable bat origin. *Nature*. 2020;579: 270–273.
650 doi:10.1038/s41586-020-2012-7
- 651 5. Wacharapluesadee S, Tan CW, Maneeorn P, Duengkae P, Zhu F, Joyjinda Y, et al. Evidence for
652 SARS-CoV-2 related coronaviruses circulating in bats and pangolins in Southeast Asia. *Nature*
653 *Communications*. 2021;12: 972. doi:10.1038/s41467-021-21240-1
- 654 6. Hul V, Delaune D, Karlsson EA, Hassanin A, Tey PO, Baidaliuk A, et al. A novel SARS-CoV-2
655 related coronavirus in bats from Cambodia. *bioRxiv*. 2021; 2021.01.26.428212.
656 doi:10.1101/2021.01.26.428212
- 657 7. Banerjee A, Kulcsar K, Misra V, Frieman M, Mossman K. Bats and Coronaviruses. *Viruses*.
658 2019;11. doi:10.3390/v11010041
- 659 8. Frutos R, Serra-Cobo J, Pinault L, Lopez Roig M, Devaux CA. Emergence of Bat-Related
660 Betacoronaviruses: Hazard and Risks. *Front Microbiol*. 2021;12.
661 doi:10.3389/fmicb.2021.591535
- 662 9. Lecis R, Mucedda M, Pidinchedda E, Pittau M, Alberti A. Molecular identification of
663 Betacoronavirus in bats from Sardinia (Italy): first detection and phylogeny. *Virus Genes*.
664 2019;55: 60–67. doi:10.1007/s11262-018-1614-8

- 665 10. De Benedictis P, Marciano S, Scaravelli D, Priori P, Zecchin B, Capua I, et al. Alpha and lineage
666 C betaCoV infections in Italian bats. *Virus Genes*. 2014;48: 366–371. doi:10.1007/s11262-013-
667 1008-x
- 668 11. Lee S, Jo S-D, Son K, An I, Jeong J, Wang S-J, et al. Genetic Characteristics of Coronaviruses
669 from Korean Bats in 2016. *Microb Ecol*. 2018;75: 174–182. doi:10.1007/s00248-017-1033-8
- 670 12. Falcón A, Vázquez-Morón S, Casas I, Aznar C, Ruiz G, Pozo F, et al. Detection of alpha and
671 betacoronaviruses in multiple Iberian bat species. *Arch Virol*. 2011;156: 1883.
672 doi:10.1007/s00705-011-1057-1
- 673 13. Patterson EI, Elia G, Grassi A, Giordano A, Desario C, Medardo M, et al. Evidence of exposure
674 to SARS-CoV-2 in cats and dogs from households in Italy. *Nature Communications*. 2020;11:
675 6231. doi:10.1038/s41467-020-20097-0
- 676 14. Koopmans M. SARS-CoV-2 and the human-animal interface: outbreaks on mink farms. *The*
677 *Lancet Infectious Diseases*. 2021;21: 18–19. doi:10.1016/S1473-3099(20)30912-9
- 678 15. Olival KJ, Cryan PM, Amman BR, Baric RS, Blehert DS, Brook CE, et al. Possibility for reverse
679 zoonotic transmission of SARS-CoV-2 to free-ranging wildlife: A case study of bats. Lakdawala
680 S, editor. *PLoS Pathog*. 2020;16: e1008758. doi:10.1371/journal.ppat.1008758
- 681 16. Lu R, Zhao X, Li J, Niu P, Yang B, Wu H, et al. Genomic characterisation and epidemiology of
682 2019 novel coronavirus: implications for virus origins and receptor binding. *The Lancet*.
683 2020;395: 565–574. doi:10.1016/S0140-6736(20)30251-8
- 684 17. Hoffmann M, Kleine-Weber H, Schroeder S, Krüger N, Herrler T, Erichsen S, et al. SARS-CoV-
685 2 Cell Entry Depends on ACE2 and TMPRSS2 and Is Blocked by a Clinically Proven Protease
686 Inhibitor. *Cell*. 2020;181: 271-280.e8. doi:10.1016/j.cell.2020.02.052
- 687 18. Ge X-Y, Li J-L, Yang X-L, Chmura AA, Zhu G, Epstein JH, et al. Isolation and characterization
688 of a bat SARS-like coronavirus that uses the ACE2 receptor. *Nature*. 2013;503: 535–538.
689 doi:10.1038/nature12711
- 690 19. Murgolo N, Therien AG, Howell B, Klein D, Koeplinger K, Lieberman LA, et al. SARS-CoV-2
691 tropism, entry, replication, and propagation: Considerations for drug discovery and development.
692 *PLOS Pathogens*. 2021;17: e1009225. doi:10.1371/journal.ppat.1009225

- 693 20. Damas J, Hughes GM, Keough KC, Painter CA, Persky NS, Corbo M, et al. Broad host range of
694 SARS-CoV-2 predicted by comparative and structural analysis of ACE2 in vertebrates. PNAS.
695 2020;117: 22311–22322. doi:10.1073/pnas.2010146117
- 696 21. Li Y, Wang H, Tang X, Fang S, Ma D, Du C, et al. SARS-CoV-2 and Three Related
697 Coronaviruses Utilize Multiple ACE2 Orthologs and Are Potently Blocked by an Improved
698 ACE2-Ig. J Virol. 2020;94. doi:10.1128/JVI.01283-20
- 699 22. Yan H, Jiao H, Liu Q, Zhang Z, Xiong Q, Wang B-J, et al. ACE2 receptor usage reveals
700 variation in susceptibility to SARS-CoV and SARS-CoV-2 infection among bat species. Nature
701 Ecology & Evolution. 2021; 1–9. doi:10.1038/s41559-021-01407-1
- 702 23. Conceicao C, Thakur N, Human S, Kelly JT, Logan L, Bialy D, et al. The SARS-CoV-2 Spike
703 protein has a broad tropism for mammalian ACE2 proteins. PLOS Biology. 2020;18: e3001016.
704 doi:10.1371/journal.pbio.3001016
- 705 24. Liu K, Tan S, Niu S, Wang J, Wu L, Sun H, et al. Cross-species recognition of SARS-CoV-2 to
706 bat ACE2. Proc Natl Acad Sci U S A. 2021;118. doi:10.1073/pnas.2020216118
- 707 25. Chu H, Chan JF-W, Yuen TT-T, Shuai H, Yuan S, Wang Y, et al. Comparative tropism,
708 replication kinetics, and cell damage profiling of SARS-CoV-2 and SARS-CoV with
709 implications for clinical manifestations, transmissibility, and laboratory studies of COVID-19: an
710 observational study. The Lancet Microbe. 2020;1: e14–e23. doi:10.1016/S2666-5247(20)30004-
711 5
- 712 26. Harcourt J, Tamin A, Lu X, Kamili S, Sakthivel SK, Murray J, et al. Severe Acute Respiratory
713 Syndrome Coronavirus 2 from Patient with Coronavirus Disease, United States. Emerg Infect
714 Dis. 2020;26: 1266–1273. doi:10.3201/eid2606.200516
- 715 27. Lau SKP, Wong ACP, Luk HKH, Li KSM, Fung J, He Z, et al. Early Release - Differential
716 Tropism of SARS-CoV and SARS-CoV-2 in Bat Cells - Volume 26, Number 12—December
717 2020 - Emerging Infectious Diseases journal - CDC. [cited 17 Sep 2020].
718 doi:10.3201/eid2612.202308
- 719 28. Zhou J, Li C, Liu X, Chiu MC, Zhao X, Wang D, et al. Infection of bat and human intestinal
720 organoids by SARS-CoV-2. Nat Med. 2020;26: 1077–1083. doi:10.1038/s41591-020-0912-6

- 721 29. Schlottau K, Rissmann M, Graaf A, Schön J, Sehl J, Wylezich C, et al. SARS-CoV-2 in fruit
722 bats, ferrets, pigs, and chickens: an experimental transmission study. *The Lancet Microbe*.
723 2020;1: e218–e225. doi:10.1016/S2666-5247(20)30089-6
- 724 30. Banerjee A, Misra V, Schountz T, Baker ML. Tools to study pathogen-host interactions in bats.
725 *Virus Research*. 2018;248: 5–12. doi:10.1016/j.virusres.2018.02.013
- 726 31. Ar Gouilh M, Puechmaille SJ, Diancourt L, Vandebogaert M, Serra-Cobo J, Lopez Roïg M, et
727 al. SARS-CoV related Betacoronavirus and diverse Alphacoronavirus members found in western
728 old-world. *Virology*. 2018;517: 88–97. doi:10.1016/j.virol.2018.01.014
- 729 32. Dominguez SR, O’Shea TJ, Oko LM, Holmes KV. Detection of Group 1 Coronaviruses in Bats
730 in North America. *Emerg Infect Dis*. 2007;13: 1295–1300. doi:10.3201/eid1309.070491
- 731 33. Mendenhall IH, Kerimbayev AA, Strochkov VM, Sultankulova KT, Kopeyev SK, Su YCF, et al.
732 Discovery and Characterization of Novel Bat Coronavirus Lineages from Kazakhstan. *Viruses*.
733 2019;11. doi:10.3390/v11040356
- 734 34. Ogando NS, Dalebout TJ, Zevenhoven-Dobbe JC, Limpens RWAL, van der Meer Y, Caly L, et
735 al. SARS-coronavirus-2 replication in Vero E6 cells: replication kinetics, rapid adaptation and
736 cytopathology. *J Gen Virol*. 2020;101: 925–940. doi:10.1099/jgv.0.001453
- 737 35. Richter M, Reimann I, Schirrmeier H, Kirkland PD, Beer M. The viral envelope is not sufficient
738 to transfer the unique broad cell tropism of Bungowannah virus to a related pestivirus. *Journal of*
739 *General Virology*,. 2014;95: 2216–2222. doi:10.1099/vir.0.065995-0
- 740 36. He X, Korytář T, Zhu Y, Pikula J, Bandouchova H, Zukal J, et al. Establishment of Myotis
741 myotis Cell Lines - Model for Investigation of Host-Pathogen Interaction in a Natural Host for
742 Emerging Viruses. *PLOS ONE*. 2014;9: e109795. doi:10.1371/journal.pone.0109795
- 743 37. Puelles VG, Lütgehetmann M, Lindenmeyer MT, Sperhake JP, Wong MN, Allweiss L, et al.
744 Multiorgan and Renal Tropism of SARS-CoV-2. *New England Journal of Medicine*. 2020;383:
745 590–592. doi:10.1056/NEJMc2011400
- 746 38. Altmann DM, Boyton RJ, Beale R. Immunity to SARS-CoV-2 variants of concern. *Science*.
747 2021;371: 1103–1104. doi:10.1126/science.abg7404

- 748 39. Davies NG, Abbott S, Barnard RC, Jarvis CI, Kucharski AJ, Munday JD, et al. Estimated
749 transmissibility and impact of SARS-CoV-2 lineage B.1.1.7 in England. *Science*. 2021;372.
750 doi:10.1126/science.abg3055
- 751 40. Montagutelli X, Prot M, Levillayer L, Salazar EB, Jouvion G, Conquet L, et al. The B.1.351 and
752 P.1 variants extend SARS-CoV-2 host range to mice. *bioRxiv*. 2021; 2021.03.18.436013.
753 doi:10.1101/2021.03.18.436013
- 754 41. Onabajo OO, Banday AR, Stanifer ML, Yan W, Obajemu A, Santer DM, et al. Interferons and
755 viruses induce a novel truncated ACE2 isoform and not the full-length SARS-CoV-2 receptor.
756 *Nature Genetics*. 2020;52: 1283–1293. doi:10.1038/s41588-020-00731-9
- 757 42. Allen JD, Watanabe Y, Chawla H, Newby ML, Crispin M. Subtle Influence of ACE2 Glycan
758 Processing on SARS-CoV-2 Recognition. *Journal of Molecular Biology*. 2021;433: 166762.
759 doi:10.1016/j.jmb.2020.166762
- 760 43. Buchrieser J, Dufloo J, Hubert M, Monel B, Planas D, Rajah MM, et al. Syncytia formation by
761 SARS-CoV-2-infected cells. *EMBO J*. 2021;40: e107405. doi:10.15252/embj.2020107405
- 762 44. Triana S, Metz-Zumaran C, Ramirez C, Kee C, Doldan P, Shahraz M, et al. Single-cell analyses
763 reveal SARS-CoV-2 interference with intrinsic immune response in the human gut. *Molecular*
764 *Systems Biology*. 2021;17: e10232. doi:10.15252/msb.202110232
- 765 45. Clausen TM, Sandoval DR, Spliid CB, Pihl J, Perrett HR, Painter CD, et al. SARS-CoV-2
766 Infection Depends on Cellular Heparan Sulfate and ACE2. *Cell*. 2020;183: 1043-1057.e15.
767 doi:10.1016/j.cell.2020.09.033
- 768 46. Zhang Q, Chen CZ, Swaroop M, Xu M, Wang L, Lee J, et al. Heparan sulfate assists SARS-
769 CoV-2 in cell entry and can be targeted by approved drugs in vitro. *Cell Discovery*. 2020;6: 1–
770 14. doi:10.1038/s41421-020-00222-5
- 771 47. Shaw AE, Hughes J, Gu Q, Behdenna A, Singer JB, Dennis T, et al. Fundamental properties of
772 the mammalian innate immune system revealed by multispecies comparison of type I interferon
773 responses. Malik H, editor. *PLoS Biol*. 2017;15: e2004086. doi:10.1371/journal.pbio.2004086

- 774 48. Zhou S, Butler-Laporte G, Nakanishi T, Morrison DR, Afilalo J, Afilalo M, et al. A Neanderthal
775 OAS1 isoform protects individuals of European ancestry against COVID-19 susceptibility and
776 severity. *Nature Medicine*. 2021;27: 659–667. doi:10.1038/s41591-021-01281-1
- 777 49. Yin X, Riva L, Pu Y, Martin-Sancho L, Kanamune J, Yamamoto Y, et al. MDA5 Governs the
778 Innate Immune Response to SARS-CoV-2 in Lung Epithelial Cells. *Cell Rep*. 2021;34: 108628.
779 doi:10.1016/j.celrep.2020.108628
- 780 50. Rebendenne A, Valadão ALC, Tauziet M, Maarifi G, Bonaventure B, McKellar J, et al. SARS-
781 CoV-2 Triggers an MDA-5-Dependent Interferon Response Which Is Unable To Control
782 Replication in Lung Epithelial Cells. *Journal of Virology*. 2021;95. doi:10.1128/JVI.02415-20
- 783 51. Blanco-Melo D, Nilsson-Payant BE, Liu W-C, Uhl S, Hoagland D, Møller R, et al. Imbalanced
784 Host Response to SARS-CoV-2 Drives Development of COVID-19. *Cell*. 2020;181: 1036-
785 1045.e9. doi:10.1016/j.cell.2020.04.026
- 786 52. Zheng M, Karki R, Williams EP, Yang D, Fitzpatrick E, Vogel P, et al. TLR2 senses the SARS-
787 CoV-2 envelope protein to produce inflammatory cytokines. *Nature Immunology*. 2021; 1–10.
788 doi:10.1038/s41590-021-00937-x
- 789 53. Ren L, Wu C, Guo L, Yao J, Wang C, Xiao Y, et al. Single-cell transcriptional atlas of the
790 Chinese horseshoe bat (*Rhinolophus sinicus*) provides insight into the cellular mechanisms
791 which enable bats to be viral reservoirs. *Cell Biology*; 2020 Jun. doi:10.1101/2020.06.30.175778
- 792 54. Straková P, Dufkova L, Širmarová J, Salát J, Bartonička T, Klempa B, et al. Novel hantavirus
793 identified in European bat species *Nyctalus noctula*. *Infect Genet Evol*. 2017;48: 127–130.
794 doi:10.1016/j.meegid.2016.12.025
- 795 55. Kurth A, Kohl C, Brinkmann A, Ebinger A, Harper JA, Wang L-F, et al. Novel Paramyxoviruses
796 in Free-Ranging European Bats. *PLoS One*. 2012;7. doi:10.1371/journal.pone.0038688
- 797 56. Sun K, Gu L, Ma L, Duan Y. Atlas of ACE2 gene expression reveals novel insights into
798 transmission of SARS-CoV-2. *Heliyon*. 2021;7: e05850. doi:10.1016/j.heliyon.2020.e05850
- 799 57. Hikmet F, Méar L, Edvinsson Å, Micke P, Uhlén M, Lindskog C. The protein expression profile
800 of ACE2 in human tissues. *Molecular Systems Biology*. 2020;16: e9610.
801 doi:10.15252/msb.20209610

- 802 58. Ghosh S, Dellibovi-Ragheb TA, Kerviel A, Pak E, Qiu Q, Fisher M, et al. β -Coronaviruses Use
803 Lysosomes for Egress Instead of the Biosynthetic Secretory Pathway. *Cell*. 2020;183: 1520-
804 1535.e14. doi:10.1016/j.cell.2020.10.039
- 805 59. Cifuentes-Muñoz N, Dutch RE, Cattaneo R. Direct cell-to-cell transmission of respiratory
806 viruses: The fast lanes. *PLOS Pathogens*. 2018;14: e1007015. doi:10.1371/journal.ppat.1007015
- 807 60. Qian Z, Dominguez SR, Holmes KV. Role of the Spike Glycoprotein of Human Middle East
808 Respiratory Syndrome Coronavirus (MERS-CoV) in Virus Entry and Syncytia Formation. *PLOS*
809 *ONE*. 2013;8: e76469. doi:10.1371/journal.pone.0076469
- 810 61. Bussani R, Schneider E, Zentilin L, Collesi C, Ali H, Braga L, et al. Persistence of viral RNA,
811 pneumocyte syncytia and thrombosis are hallmarks of advanced COVID-19 pathology.
812 *EBioMedicine*. 2020;61: 103104. doi:10.1016/j.ebiom.2020.103104
- 813 62. Hayn M, Hirschenberger M, Koepke L, Nchioua R, Straub JH, Klute S, et al. Systematic
814 Functional Analysis of SARS-CoV-2 Proteins Uncovers Viral Innate Immune Antagonists and
815 Remaining Vulnerabilities. *Cell Reports*. 2021; 109126. doi:10.1016/j.celrep.2021.109126
- 816 63. Stukalov A, Girault V, Grass V, Karayel O, Bergant V, Urban C, et al. Multilevel proteomics
817 reveals host perturbations by SARS-CoV-2 and SARS-CoV. *Nature*. 2021. doi:10.1038/s41586-
818 021-03493-4
- 819 64. Banerjee A, Falzarano D, Rapin N, Lew J, Misra V. Interferon Regulatory Factor 3-Mediated
820 Signaling Limits Middle-East Respiratory Syndrome (MERS) Coronavirus Propagation in Cells
821 from an Insectivorous Bat. *Viruses*. 2019;11. doi:10.3390/v11020152
- 822 65. Hall JS, Knowles S, Nashold SW, Ip HS, Leon AE, Rocke T, et al. Experimental challenge of a
823 North American bat species, big brown bat (*Eptesicus fuscus*), with SARS-CoV-2.
824 *Transboundary and Emerging Diseases*. n/a. doi:https://doi.org/10.1111/tbed.13949
- 825 66. De La Cruz-Rivera PC, Kanchwala M, Liang H, Kumar A, Wang L-F, Xing C, et al. The IFN
826 Response in Bats Displays Distinctive IFN-Stimulated Gene Expression Kinetics with Atypical
827 RNASEL Induction. *J. Immunol.* 2018;200: 209–217. doi:10.4049/jimmunol.1701214

- 828 67. Zhou P, Tachedjian M, Wynne JW, Boyd V, Cui J, Smith I, et al. Contraction of the type I IFN
829 locus and unusual constitutive expression of IFN- α in bats. *PNAS*. 2016;113: 2696–2701.
830 doi:10.1073/pnas.1518240113
- 831 68. Banerjee A, Baker ML, Kulcsar K, Misra V, Plowright R, Mossman K. Novel Insights Into
832 Immune Systems of Bats. *Front Immunol*. 2020;11: 26. doi:10.3389/fimmu.2020.00026
- 833 69. Banerjee A, Zhang X, Yip A, Schulz KS, Irving AT, Bowdish D, et al. Positive Selection of a
834 Serine Residue in Bat IRF3 Confers Enhanced Antiviral Protection. *iScience*. 2020;23: 100958.
835 doi:10.1016/j.isci.2020.100958
- 836 70. Zhou P, Cowled C, Mansell A, Monaghan P, Green D, Wu L, et al. IRF7 in the Australian Black
837 Flying Fox, *Pteropus alecto*: Evidence for a Unique Expression Pattern and Functional
838 Conservation. Fugmann SD, editor. *PLoS ONE*. 2014;9: e103875.
839 doi:10.1371/journal.pone.0103875
- 840 71. Brook CE, Boots M, Chandran K, Dobson AP, Drostén C, Graham AL, et al. Accelerated viral
841 dynamics in bat cell lines, with implications for zoonotic emergence. *eLife*. 2020;9: e48401.
842 doi:10.7554/eLife.48401
- 843 72. Irving AT, Ahn M, Goh G, Anderson DE, Wang L-F. Lessons from the host defences of bats, a
844 unique viral reservoir. *Nature*. 2021;589: 363–370. doi:10.1038/s41586-020-03128-0
- 845 73. Glennon NB, Jabado O, Lo MK, Shaw ML. Transcriptome Profiling of the Virus-Induced Innate
846 Immune Response in *Pteropus vampyrus* and Its Attenuation by Nipah Virus Interferon
847 Antagonist Functions. *Journal of Virology*. 2015;89: 17.
- 848 74. Yohe LR, Devanna P, Davies KTJ, Potter JHT, Rossiter SJ, Teeling EC, et al. Tissue Collection
849 of Bats for -Omics Analyses and Primary Cell Culture. *J Vis Exp*. 2019. doi:10.3791/59505
- 850 75. Aurine N, Baquerre C, Gaudino M, Jean C, Dumont C, Rival-Gervier S, et al. Reprogrammed
851 *Pteropus* Bat Stem Cells Present Distinct Immune Signature and are Highly Permissive for
852 Henipaviruses. *bioRxiv*. 2019; 846410. doi:10.1101/846410
- 853 76. Pikula J, Bandouchova H, Kovacova V, Linhart P, Piatek V, Zukal J. Reproduction of Rescued
854 Vespertilionid Bats (*Nyctalus noctula*) in Captivity: Veterinary and Physiologic Aspects. *Vet
855 Clin North Am Exot Anim Pract*. 2017;20: 665–677. doi:10.1016/j.cvex.2016.11.013

856 77. Ramakrishnan MA. Determination of 50% endpoint titer using a simple formula. *World J Virol.*
857 2016;5: 85–86. doi:10.5501/wjv.v5.i2.85

858

859

860 **Author contributions.** S.M.A., L.D. and N.J. designed the study. S.M.A, F.S., M.C., De.P. and D.S.L.
861 performed experiments. J.B. generated A549-hACE2 cells and hACE2 lentiviral vectors. J.P., M.N.
862 and V.S. generated the Nn cell lines. J.S.C., Do.P. J.Z. and J.P. organized field trips and collected bat
863 wing biopsies. L.D. generated primary bat cells. S.M.A., F.S., M.C., De.P, L.D. and N.J. analyzed the
864 data. O.S., L.D. and N.J. supervised the work. S.M.A., F.S. and N.J. wrote the manuscript. All authors
865 edited the manuscript.

866

867 **Competing interests.** The authors declare that no competing interests exist.

868

869 **Figure legends**

870

871 **Fig 1. Resistance to SARS-CoV-2 infection in selected bat cell lines.** **A**, Primary bat cells derived
872 from wing tissues from four different species, as well as Vero E6 cells, were left uninfected (Mock) or
873 were infected with SARS-CoV-2 at a MOI of 1 for 24 hours and analyzed via flow cytometry for viral
874 spike (S) protein expression. **B**, Representative dot plots of selected cells. Data points represent three
875 technical replicates. **C**, Bat cell lines from four different species, as well as Caco TC7 human intestine
876 and A549 human lung epithelial cells, were left uninfected (Mock) or were infected with SARS-CoV-
877 2 at a MOI of 1 for 24 hours and analyzed via flow cytometry for S expression. **D**, Representative dot
878 plots of selected cells. Data points represent three independent experiments with the exception of
879 A549, FLN-ID and FLN-R cells, where data points represent three technical replicates.

880

881 **Fig. 2. Expression of endogenous ACE2 or ectopically-expressed hACE2 in bat cell lines.** **a**,
882 Quantification of copy numbers per μg of total cellular RNA of endogenously expressed ACE2 in
883 indicated bat cell lines via qPCR analysis. **B**, **C**, **D**, Indicated bat and human cell lines were stably
884 transduced with a lentivirus vector expressing the hACE2 gene and selected with blasticidin treatment.
885 Human Caco-TC7 intestine cell line served as non-transduced control. **B**, Amount of ectopically-
886 expressed hACE2 gene in each cell line was measured by qPCR analysis and indicated as gene copy
887 number per μg of total cellular RNA. **C**, Whole-cell lysates were analyzed by Western blotting with
888 antibodies against the indicated proteins. Western blots are representative of two independent
889 experiments. **D**, Ectopic hACE2 expression levels of transduced cell lines analyzed via flow cytometry
890 with anti-hACE antibody staining. (a,b,d) Data points represent three independent experiments. (A, B)
891 dotted line indicated limit of detection in qPCR assays.

892

893 **Fig. 3. Time-lapse microscopy of *Myotis myotis* and *Eptesicus serotinus* brain cells during SARS-**
894 **CoV-2 infection.** MmBr-ACE2 (**A**) and FLG-ID-ACE2 (**B**) cells were left uninfected (Mock) or were
895 infected with SARS-CoV-2 at a MOI of 1 in media containing propidium iodide (PI) as cell death

896 marker. Images were taken every 10 minutes. Quantification of cell death (area of PI) displayed on the
897 right of corresponding video cutouts. Results are mean \pm SD from three fields per condition.

898

899 **Fig. 4. Expression of hACE2 allows efficient replication of SARS-CoV-2 in *Myotis myotis* and**

900 ***Eptesicus serotinus* cells.** Transduced bat cell lines were left uninfected (Mock) or were infected with

901 SARS-CoV-2 at a MOI of 1, with the exception of MmBr cells that were infected at a MOI of 0.04. **A,**

902 The relative amounts of cell-associated viral RNA were determined by qPCR analysis and are

903 expressed as genome equivalents (GE) per μ g of total cellular RNA at different time post-infection.

904 All results are expressed as fold-increases relative to uninfected cells. **B, C,** Infected cells were stained

905 at 24 hpi with anti-SARS-CoV-2 S protein (red) and/or anti-hACE2 antibodies (green). Nuclei were

906 stained with Nucblue (blue). Scale bar, 10 μ m. **D, E,** The percentages of the indicated cells that

907 contained SARS-CoV-2 S proteins (d) or hACE2 (e) were determined by flow cytometric analysis at

908 24 hpi. **F,** The presence of extracellular infectious viruses in the culture medium of the indicated cells

909 was determined by TCID₅₀ assays with Vero E6 cells at 24 and 48 hpi. Dashed lines indicate the limit

910 of detection. (a, d, e, f) Data points represent three independent experiments. Statistical test: (a)

911 Dunnett's multiple comparison test on a two-way ANOVA analysis (n.s: not significant; * p-value <

912 0.05, ** p-value < 0.01, *** p-value < 0.001, **** p-value < 0.0001); (e, f) Šídák's multiple

913 comparisons test on a two-way ANOVA analysis (n.s: not significant, * p-value < 0.05, ** p-value <

914 0.01, *** p-value < 0.001, **** p-value < 0.0001).

915

916 **Fig. 5. Infectious particles are produced by MmBr-ACE2 cells but not released.** A549-ACE2 and

917 MmNep-ACE2 cells were left uninfected (Mock) or were infected at a MOI of 1 for 24 hours. MmBr-

918 ACE2 cells were left uninfected (Mock) or were infected at a MOI of 0.04 for 24 hours. **A,** The

919 percentages of the indicated cells that contained SARS-CoV-2 S proteins were determined by flow

920 cytometric analysis. **B,** The presence of extracellular infectious viruses in the culture medium of the

921 indicated cells was determined by TCID₅₀ assays performed on Vero E6 cells. Supernatants were either

922 clarified or purified by ultracentrifugation. Alternatively, cell-associated infectious virions were

923 titrated on Vero E6 cells from whole cell lysates. Data points represent three independent experiments.

924 Statistical test: Dunnett's multiple comparison test on a two-way ANOVA analysis (n.s.: not
925 significant, * p-value < 0.05, ** p-value < 0.01, *** p-value < 0.001, **** p-value < 0.0001).

926

927 **Fig. 6. An abortive entry route exists in bat and human cells. A,** Cells were incubated with SARS-
928 CoV-2 at a MOI of 1 for 1 hour on ice to allow viral attachment. After extensive washing, a portion of
929 the cells was lysed ("on ice") and the remaining cells were incubated for 2 or 6 hours at 37°C to permit
930 viral internalization. After the incubation period, these cells were lysed after 30 min trypsinization to
931 remove bound viruses from the cell surface ("2h", "6h"). **B,** A 30 min trypsinization step was added
932 after the initial incubation on ice ("on ice + trypsin"). The "on ice" and "2h" conditions are the same
933 as (a). **A, B** The relative amounts of cell-associated viral RNA were determined by qPCR analysis and
934 are expressed as genome equivalents (GE) per µg of total cellular RNA. Data points represent three
935 independent experiments. Statistical test: Dunnett's multiple comparison test on a two-way ANOVA
936 analysis (n.s.: not significant, * p-value < 0.05, ** p-value < 0.01, *** p-value < 0.001, **** p-value <
937 0.0001).

938

939 **Fig. 7. Viral IFN counteraction mechanisms are species-specific. A, B,** Non-transduced cell lines
940 were transfected with 250 ng low-molecular weight PolyI:C or were treated with PBS for 16 hours.
941 The relative amounts of *IFIH1* mRNA (a) and *OAS1* mRNA (b) were determined by qPCR analysis.
942 Results are expressed as fold-increases relative to unstimulated PBS-treated cells. **C, D,** Whole cell
943 lysates of infected cells (same lysates used for viral quantification in panel 4a) were analyzed via RT-
944 qPCR assays for the relative amounts of *IFIH1* mRNA (c) and *OAS1* mRNA (d). Results are
945 expressed as fold-increases relative to uninfected cells. **(A-D)** Glyceraldehyde 3-phosphate
946 dehydrogenase (GAPDH) of corresponding species was used as house-keeping gene. Data points
947 represent three independent experiments.

948

949 **Movie legends**

950

951 **Movie 1. Time-lapse microscopy of mock-infected MmBr-ACE2 cells.** MmBr-ACE2 cells were
952 seeded at 9×10^4 cells per quadrant in a μ -Dish 35 mm Quad dish (Ibidi) and cultured in fresh media
953 (2,5% FBS) containing propidium iodide the next day. Transmission and fluorescence images were
954 taken every 15 min, up to 48 h, using a Nikon BioStation IMQ, at 37°C with three fields
955 of acquisition for each condition.

956

957 **Movie 2. Time-lapse microscopy of MmBr-ACE2 cells infected with SARS-CoV-2.** MmBr-ACE2
958 cells were seeded at 9×10^4 cells per quadrant in a μ -Dish 35 mm Quad dish (Ibidi) and infected the
959 next day with SARS-CoV-2 at a MOI of 1 in culture medium (2,5% FBS) containing
960 propidium iodide. Transmission and fluorescence images were taken every 15 min, up to 48 h, using a
961 Nikon BioStation IMQ, at 37°C with three fields of acquisition for each condition.

962

963 **Movie 3. Time-lapse microscopy of mock-infected FLG-ID-ACE2 cells.** FLG-ID cells were seeded
964 at 5.4×10^4 cells per quadrant in a μ -Dish 35 mm Quad dish (Ibidi) and cultured in fresh media (2,5%
965 FBS) containing propidium iodide the next day. Transmission and fluorescence images were taken
966 every 15 min, up to 48 h, using a Nikon BioStation IMQ, at 37°C with three fields of acquisition for
967 each condition.

968

969 **Movie 4. Time-lapse microscopy of FLG-ID-ACE2 cells infected with SARS-CoV-2.** FLG-ID cells
970 were seeded at 5.4×10^4 cells per quadrant in a μ -Dish 35 mm Quad dish (Ibidi) and infected the next
971 day with SARS-CoV-2 at a MOI of 1 in culture medium (2,5% FBS) containing
972 propidium iodide. Transmission and fluorescence images were taken every 15 min, up to 48 h, using a
973 Nikon BioStation IMQ, at 37°C with three fields of acquisition for each condition.

974

975

976 **Supplementary figure legends**

977

978 **Fig. S1. Resistance to infection with SARS-CoV-2 variants (B1.351 and P1) in selected bat cell**

979 **lines. A, B)** Caco-TC7 and bat cell lines were left uninfected (Mock) or were infected with the SARS-
980 CoV-2 variants B1.351 (South Africa) and P1 (Brazil) at a MOI of 1 for 24 hours. The percentages of
981 the indicated cells that express the viral S proteins were determined by flow cytometric analysis. **C)**
982 Caco-TC7 and NnKi cells were left uninfected (Mock) or were infected with SARS-CoV-2 at a MOI
983 of 1 in the absence of FBS and in the presence of trypsin TPCK at 1 μ g/ml. The percentages of S-
984 positive cells were determined by flow cytometric analysis. Data points represent two technical
985 replicates.

986

987 **Fig. S2. Flow cytometry analysis of infected bat cells. A,** Dot plots and density plots of MmBr-

988 ACE2 cells infected with SARS-CoV-2 at a MOI of 0.04 for 24 hours. Cell granularity (SSC) is
989 displayed against size (FSC) to visualize the larger-size subpopulation of cells appearing during
990 infection. **B,** Dot plots of SARS-CoV-2 infected MmBr-ACE2 (MOI of 0.04) and FLG-ID-ACE2
991 (MOI of 1) cells for 24 hours and stained with anti-spike and anti-hACE2-647 antibodies, displayed on
992 x- and y-axes respectively, to show absence/presence of double positive cell subpopulations. (a,b)
993 Plots are representative of three independent experiments.

Figure 1

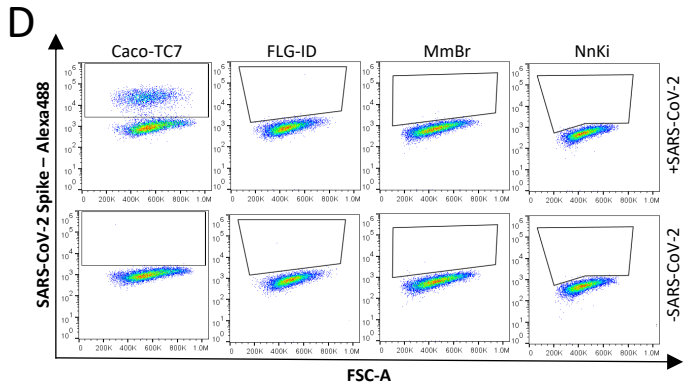
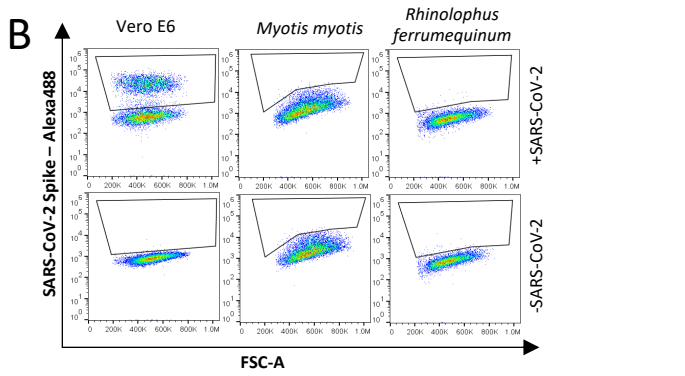
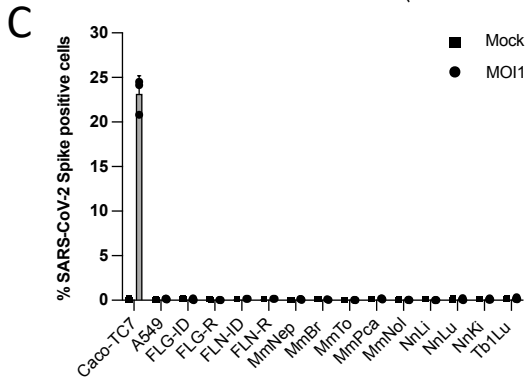
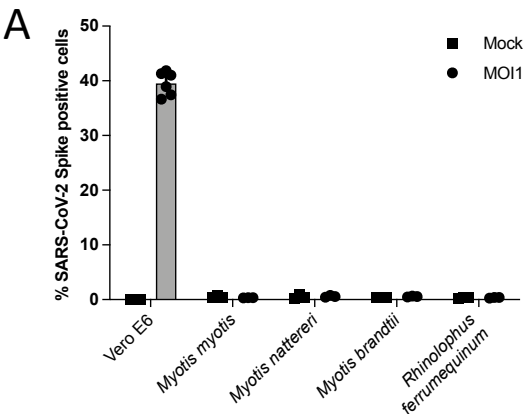


Figure 2

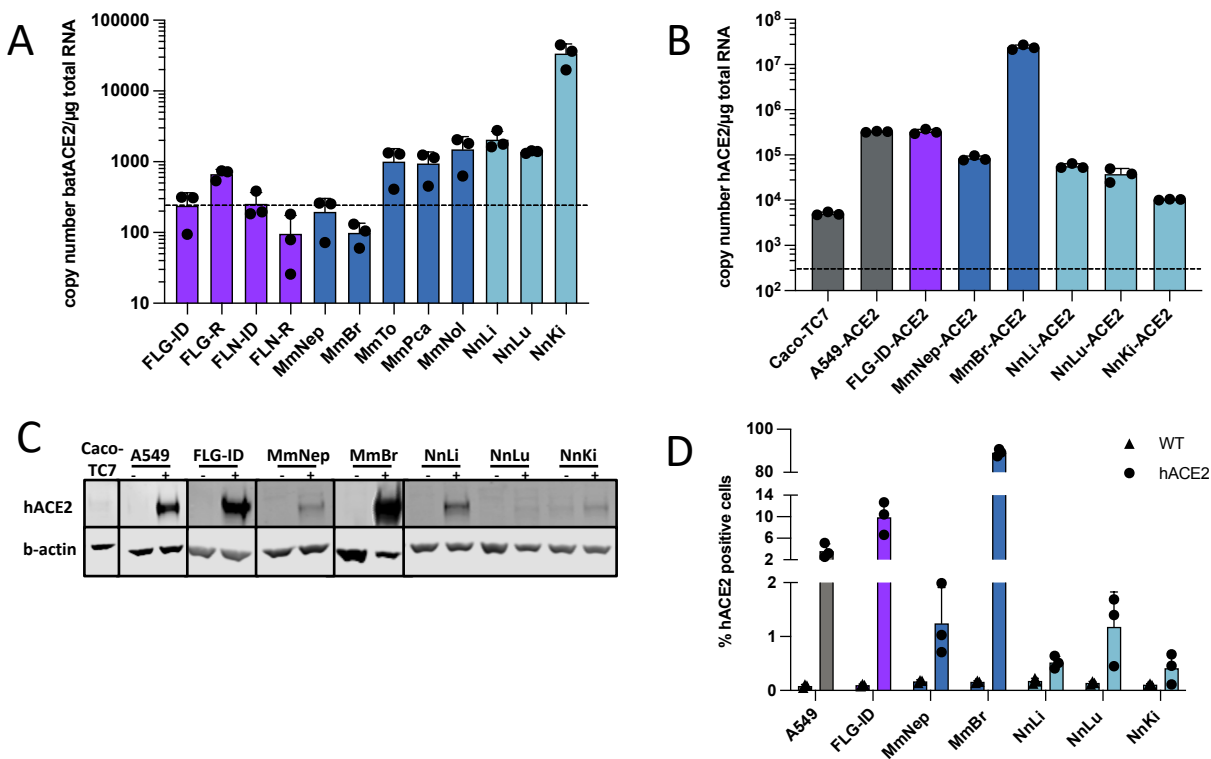


Figure 3

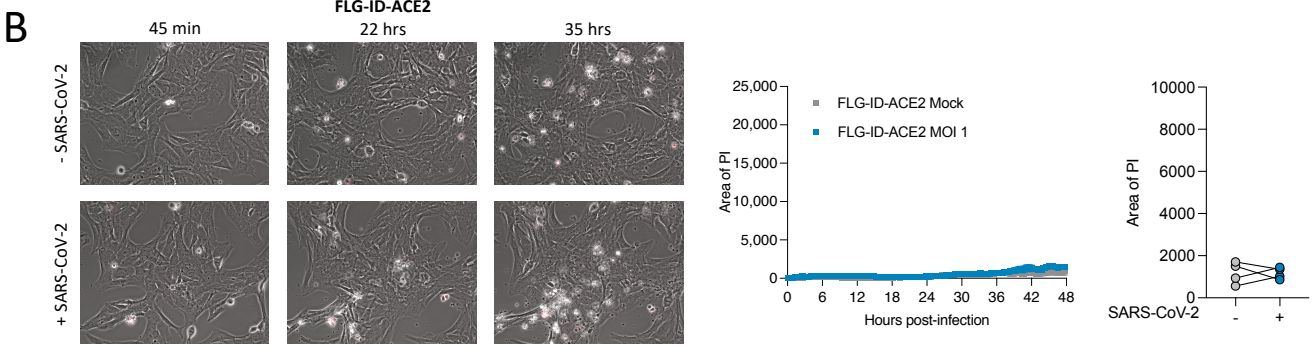
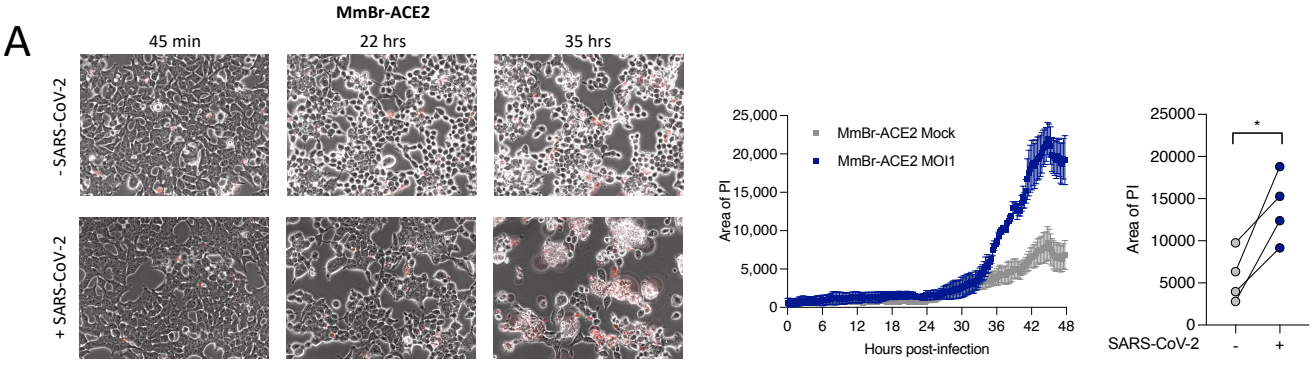


Figure 4

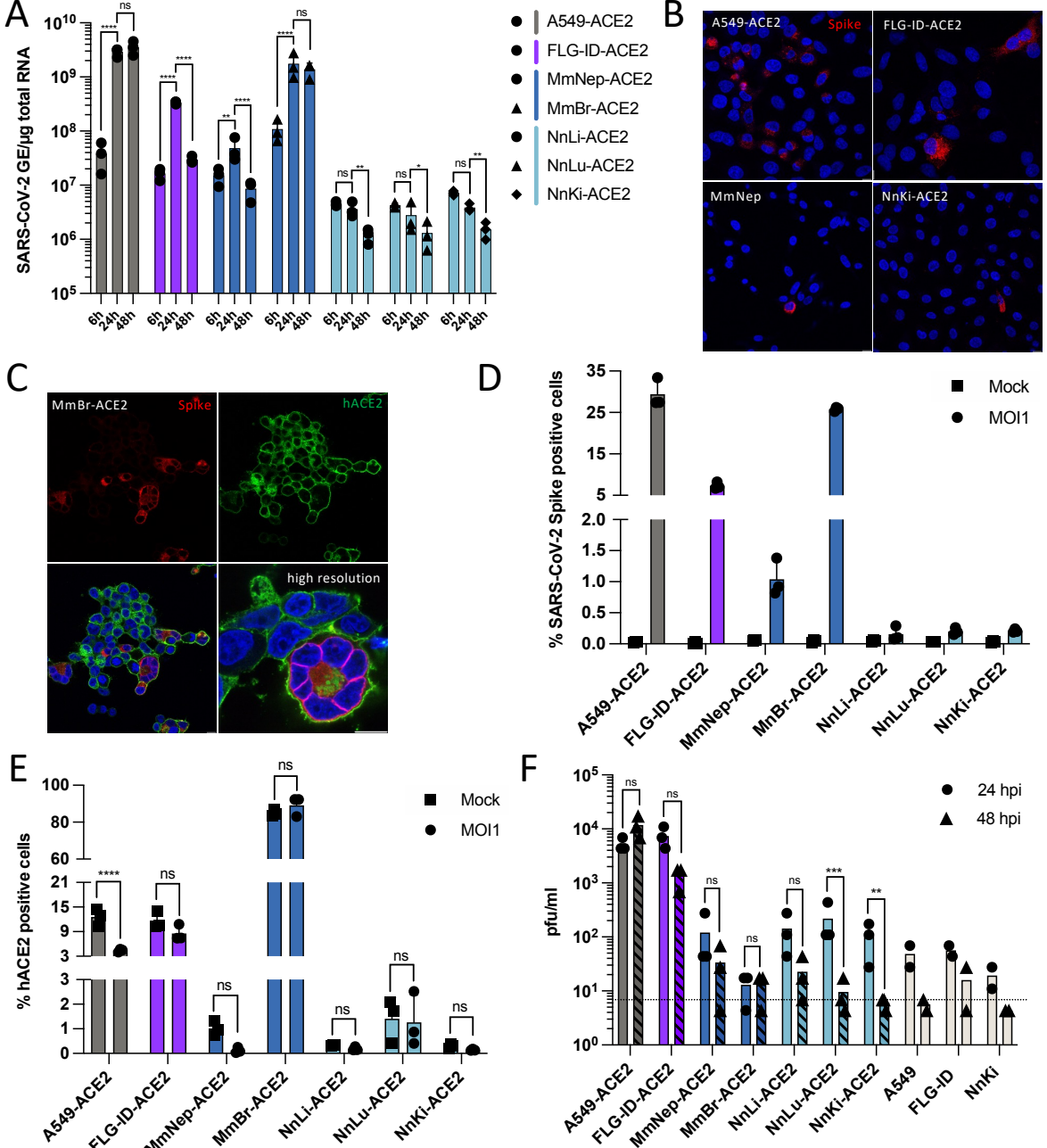
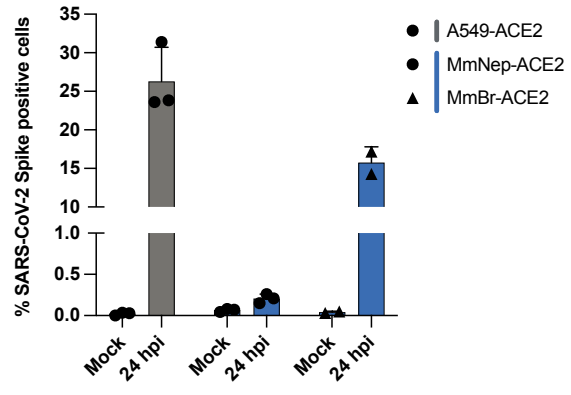


Figure 5

A



B

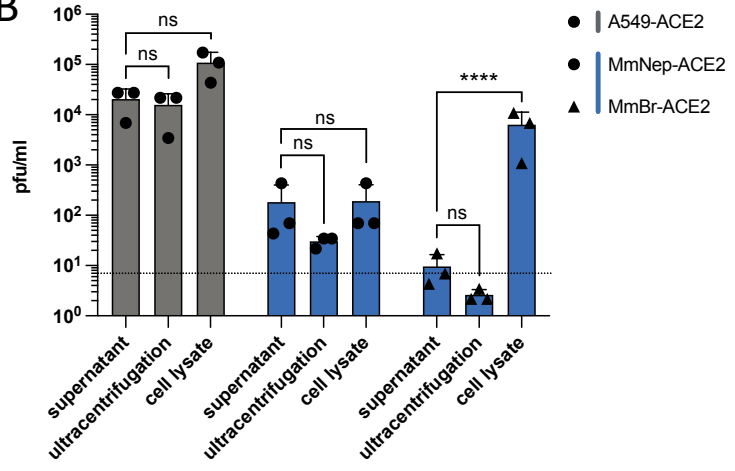


Figure 6

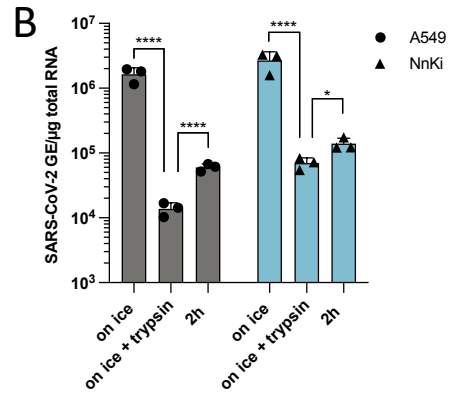
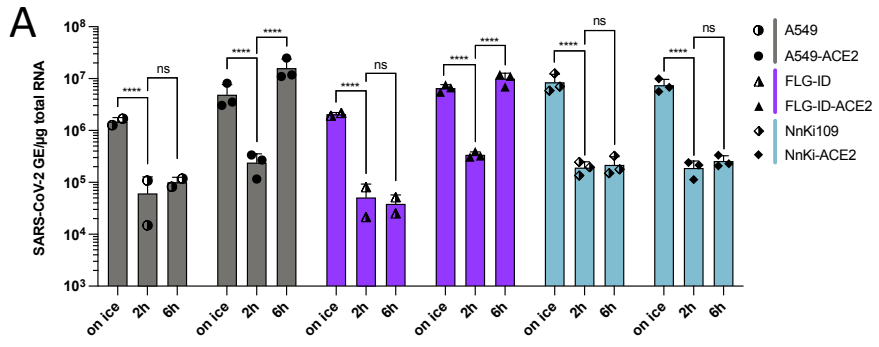


Figure 7

